minerals

MDPI

Article

The Devonian Kalarskoe Epithermal Occurrence of the Kaburchak Au-Ag Cluster in the Altai-Sayan Folded Area, Russia: Geological Setting; Mineralogical, Geochemical, and Geochronological Features

Alexander I. Chernykh [1], Polina N. Leibham [2], Lidia A. Sokolova [3,4], Olga V. Yakubovich [3,4], Maria O. Anosova [5] and Evgeny A. Naumov [2,*]

[1] PJSC Polyus, Krasina Street 3, Building 1, Moscow 123056, Russia; chernykhai@polys.com
[2] Central Research Institute of Geological Prospecting for Base and Precious Metals (TsNIGRI), Varshvskoe Shosse 129 k1, Moscow 117545, Russia; leibham@tsnigri.ru
[3] Institute of Earth Sciences, St. Petersburg University, Universitetskaya Embankment 7/9, St. Petersburg 199034, Russia; sokolovalidia@inbox.ru (L.A.S.); olya.v.yakubovich@gmail.com (O.V.Y.)
[4] Institute of Precambrian Geology and Geochronology RAS, Makarova Embankment 2, St. Petersburg 199034, Russia
[5] Vernadsky Institute of Geochemistry and Analytical Chemistry RAS, Kosygina Street 19, Moscow 119334, Russia; anosova@geokhi.ru
* Correspondence: naumov@tsnigri.ru

Abstract: Prospecting efforts to located Au mineralization within the Altai-Sayan fold area (ASFA) over previous decades have revealed that Devonian epithermal Au-Ag mineralization is more widespread than previously recognized. The preservation of this type of mineralization in Paleozoic rocks offers new prospects for the exploration of Au-Ag deposits in the underexplored region of Gornaya Shoria. The Kalarskoe epithermal Au-Ag occurrence represents Devonian epithermal mineralization within the Kaburchak cluster, Gornaya Shoria, Russia. This occurrence is confined to zones of argillic alteration that were superimposed on previously formed propylites. The argillic-altered rocks host quartz-sulfide veinlet zones. The mineralization of the Kalarskoe site is characterized by a high abundance of sulfide minerals: commonly, 5%–10%; often, up to 20%; and in some cases, up to 60%–70%. The ore minerals are represented by pyrite, arsenopyrite, sphalerite, galena, chalcopyrite, fahlores, native Au, and electrum, as well as by the sulfosalts Pb, Bi, Ag, Cu, and the tellurides of Au, Ag, and Pb. Based on mineralogical observations, at least four generations of sulfide mineral formations are distinguished within the ore occurrence. The mineralization of the Kalarskoe ore occurrence may be assigned to the intermediate sulfidation (IS) type. The results of the (U,Th)-He dating of pyrite from the pyrite-arsenopyrite massive body (pyr-3 and 4) revealed the protracted history of the mineralization in the intervals from ~399 to ~371 Ma. The obtained results substantially enhance the prospecting models for the exploration of epithermal Au-Ag deposits in the western part of the Altai-Sayan fold area (ASFA).

Keywords: epithermal Au; Au-Ag mineralization; (U-Th)/He dating; ore geochronology; pyrite

check for updates

Citation: Chernykh, A.I.; Leibham, P.N.; Sokolova, L.A.; Yakubovich, O.V.; Anosova, M.O.; Naumov, E.A. The Devonian Kalarskoe Epithermal Occurrence of the Kaburchak Au-Ag Cluster in the Altai-Sayan Folded Area, Russia: Geological Setting; Mineralogical, Geochemical, and Geochronological Features. *Minerals* **2024**, *14*, 708. https://doi.org/10.3390/min14070708

Academic Editors: Huan Li, Federica Zaccarini, Gülcan Bozkaya, David Banks and Evgeniy Naumov

Received: 13 May 2024
Revised: 1 July 2024
Accepted: 8 July 2024
Published: 12 July 2024

Copyright: © 2024 by the authors. Licensee MDPI, Basel, Switzerland. This article is an open access article distributed under the terms and conditions of the Creative Commons Attribution (CC BY) license (https://creativecommons.org/licenses/by/4.0/).

1. Introduction

The Altai-Sayan folded area (ASFA) is located in the northern part of the Central Asian fold belt. In the Altai-Sayan ore province, the middle Cambrian-Ordovician mineralization, represented primarily by abandoned Au-sulfide-quartz and Au-skarn deposits, which are related to collision granites, is well studied. Prospecting efforts regarding Au mineralization within the Altai-Sayan fold area (ASFA) over recent decades has revealed that Devonian epithermal Au-Ag mineralization is more widespread than was previously believed [1–3].

In the western part of the ASFA, there is a fragmented volcanic belt composed of Devonian volcanics and volcanogenic sedimentary rocks, intruded by numerous subvolcanic bodies. Fragments of Au-Ag mineralized volcanic rocks form grabens and troughs, which can be traced from western Altai (Novofirsov deposit), through Gornaya Shoria (Kalarskoe occurrence), to the north of Kuznetsk Alatau (Tuluyul occurrence). Among them, the most studied is the Novofirsov deposit. It holds Au reserves of more than nine tons, with an average grade of 1–2 g/t and an annual production of between 100 to 600 kg. The widespread occurrence of Au-Ag mineralization, combined with the insufficient exploration of the area, along with the economic significance of the previously discovered deposits, determine the necessity for a detailed investigation of this territory.

Herein, we present the geological structure of the Kaburchak cluster of the ASFA (Figure 1), its mineralogy and geochemistry, as well as new geochronological data. These results significantly supplement the existing materials regarding the geology of the ASFA and highlight several controversial issues.

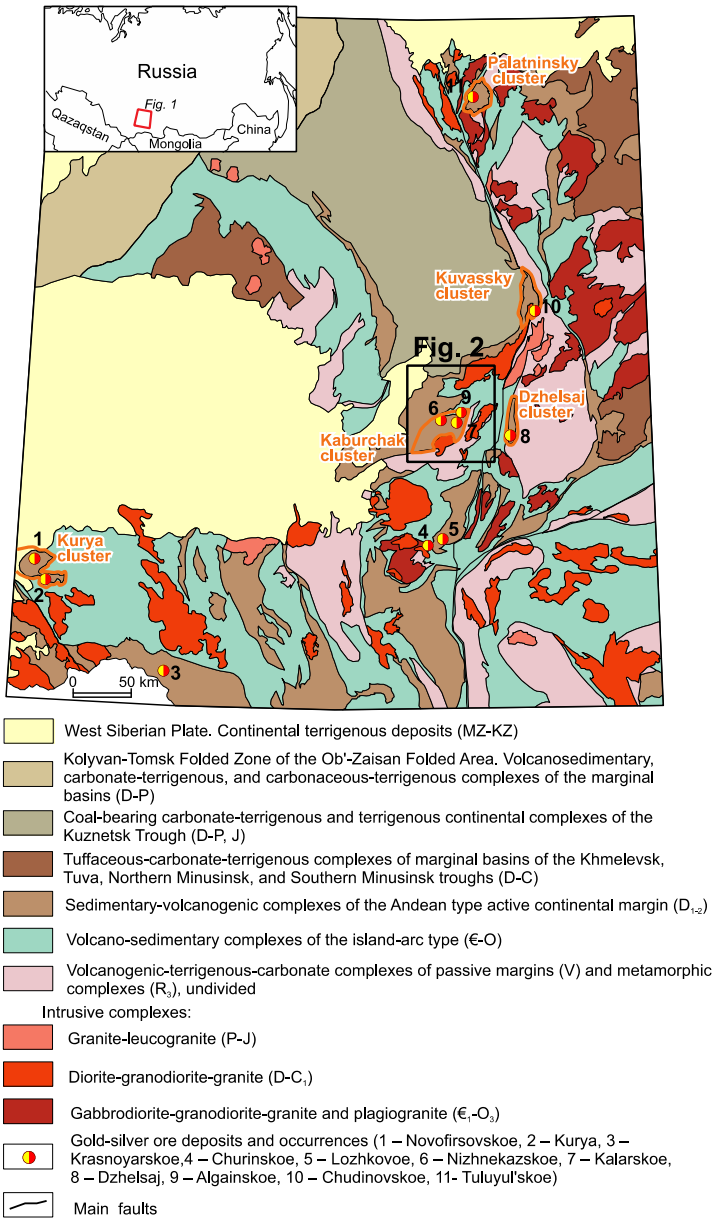


Figure 1. Schematic map showing the distribution of epithermal Au-Ag mineralization in the western segment of the ASFA (Figure 2).

2. Geological Settings and Regional Metallogeny

The western segment of ASFA is marked by an Early to Middle Devonian volcano-plutonic belt, formed under conditions of an active Andean-type margin. Permian-Triassic basalts, dolerites, and occasional granites, linked to plume magmatism, are the youngest igneous rocks in the area.

Au-Ag mineralization in the western segment of the ASFA is spatially related to the Early-Middle Devonian volcano-sedimentary and subvolcanic rocks. These volcanic rocks, along with various intrusive complexes, form a volcano-plutonic belt, which is presented in a series of disconnected volcano-tectonic troughs and grabens superimposed on the Caledonian folded basement (see Figure 1). It is assumed that these rocks were formed under the Andean-type active margin conditions [4]. The preservation of Au-Ag mineralization in the western sector of the Altai-Sayan orogenic belt is controlled by its localization within the basal horizons of Early-Middle Devonian volcanogenic sedimentary sequences, situated at the base of graben structures. This spatial confinement secures the persistence of these rocks at the modern erosion level.

The Early-Middle Devonian sequences, which host the Au-Ag mineralization, are predominantly formed by effusive rocks of felsic, intermediate, and mafic composition. Tuffs and tuffites, with interlayers of terrigenous, and in lesser amounts, clayey-carbonate sediments, are also present. The stocks, dikes, and sills of hypabyssal rocks of acid, intermediate, and less commonly, of mafic composition are widely developed within the area. In some cases, the mineralized quartz veins cut the Caledonian basement rocks, but in close proximity to the Devonian subvolcanic bodies (the Algainskoe occurrence).

Signs of Au-Ag mineralization are traced from the northwestern Altai, through Gornaya Shoria, and up to the north of the Kuznetsk Alatau ridge [5]. From west to east, the Kurya, Kaburchak, Dzhelsaj, Kuvassky, and Palatninsky Au-Ag clusters are distinguished in Figure 1. The Au-Ag mineralization of the Kuznetsk Alatau (the Palatninsky and Kuvassky clusters) is the least studied among the western ASFA. The Gornaya Shoria and Altai territory (the Kurya, Kaburchak, and Dzhelsaj clusters) were the subject of recent investigations. Previous research [1,6] and the results of geological explorations demonstrated the similarity of the Au-Ag mineralization of the western ASFA with the typical epithermal objects of the Okhotsk-Chukotka Volcanic Belt in the Far East of the Russian Federation. Analysis of the available geological and mineralogical-geochemical data suggests that the Au-Ag mineralization in the western ASFA belongs to the low sulfidation (LS), intermediate sulfidation (IS), and high sulfidation (HS) types, according to the classification by R.H. Sillitoe and J.W. Hedenquist [7]. An example of the LS type is the Novofirsovskoe deposit [5]; an example of the HS type is the Lozhkovoe occurrence [8]; and an example of the IS type is the Kalarskoe occurrence [9].

3. Geochronology

As stated earlier, the Au-Ag mineralization of the western part of the ASFA reveals a strong spatial and genetic connection with the early-middle Devonian volcanic and subvolcanic complexes located in the fragmented volcanic-plutonic belt. Mineralization-generating and mineralization-hosting volcanic rocks are interbedded with terrigenous and carbonate rocks, whose age is determined by paleontological methods as 415 to 375 Ma. The majority of rocks are with age of 405–383 Ma. Based on geological data, it is assumed that the age of Au-Ag mineralization is Early-Middle Devonian.

The age of the subvolcanic and volcanic complexes in the western part of the ASFA was studied using isotopic geochronological methods. The age of the rhyolites-porphyries, with mineralized quartz veins that host Au-Ag mineralization in the Kurya cluster, (Figure 1) was determined using the U-Pb method on zircons (SHRIMP-II). The ages vary between 373 to 382 Ma (Table 1) [5]. Obtained by the same method, the age of subvolcanic rhyolites from the Kurya occurrence is 389–393 Ma, and that of andesites is ~390 Ma. The U-Pb ages of zircons extracted from explosive Au-bearing breccia from the Kurya occurrence reveal two stages of Au-Ag mineralization, i.e., 349–359 Ma and 126 Ma [3].

Table 1. Geochronological data of Au-Ag mineralization in Altai-Sayan fold area (ASFA).

Object	Rock/Complex	Age	Method	Source
Surich-2	rhyolite porphyry/Kuyagan	382 ± 3.5	Zr U-Pb	[5]
Tolstuha mountain	quartz-diorite porphyry	378.9 ± 3.4	Zr U-Pb	[5]
Verbluzhya mountain	rhyolite porphyry/Kuyagan	372.7 ± 3.7	Zr U-Pb	[5]
Kurya occurence	Rhyolite/Sagan	389 ± 3	Zr U-Pb	[3]
		390 ± 3	Zr U-Pb	
		393 ± 3	Zr U-Pb	
	Andesite	390.5 ± 5.5	Zr U-Pb	
		~400	Zr U-Pb	
	Au-bearing breccias	349 ± 3	Zr U-Pb	
		359 ± 7	Zr U-Pb	
		126 ± 3	Zr U-Pb	
Kalarskoe occurence	Rhyolite porphyry	379.5 ± 1.6	Zr U-Pb	[10]
	Au-bearing beresites	396.2 ± 3.8	Ser Ar-Ar	[1]
	Mineralized zones (pyrite-arsenopyrite massive body)	371–399	Pyr (U,Th)-He	(this study)

U-Pb ages obtained on zircons (SHRIMP-II; VSEGEI; Saint Petersburg, Russia); Ar-Ar ages obtained on sericite (Sobolev Institute of Geology and Mineralogy RAS; Novosibirsk, Russia).

The age of the rhyolite-porphyry dike at the Kalarskoe field is 379.5 ± 1.6 Ma (zircon, U-Pb; SHRIMP-II [10]), which is close to the age of the dikes of the Kuyagan complex of the Kurya field (373–382 Ma). Ar-Ar ages of sericite from a dike of beresitized Au-Ag-bearing dacite porphyries of the Kaburchak complex revealed an age of 396.2 ± 3.8 Ma [1]. According to geological data, the age of the dikes of the Kaburchak complex is assumed to be ~400 million years, which is close to the age of the rhyolite dikes at the Kurya occurrence.

4. Au-Bearing Potential of the Kaburchak Au-Ag Cluster

The Kaburchak Au-Ag cluster, which is located within the Devonian volcano-tectonic structure of the same name (see Figures 1 and 2), was singled out in the course of the geological exploration focused on Au mineralization [11].

The Early-Middle Devonian volcano-sedimentary rocks of the Uchulen-Kazankol complex ($D_{1–2uk}$) are cut by comagmatic syenogranite-granite-leucogranite intrusions of the Kistal complex (D_{1k}) (Figure 2). The basement of the Kaburchak volcano-tectonic structure is formed by the red-colored terrigenous rocks which overlie the Vendian terrigenous-carbonate sediments of the passive continental margin and the Cambrian island-arc volcano-sedimentary rocks.

The rocks of the Kistal syenogranite-granite-leucogranite complex make up the polyphase Kistal massif in the southern segment of the Kaburchak volcano-tectonic structure. The main volume of the massif is composed of diorites and monzodiorites of the first phase. The second phase is represented by small bodies of granitoid composition, and the third phase comprises dikes and small stocks of leucogranite composition. The granites of the Kistal massif cut the volcanic rocks and are overlaid (by erosion) with the Early-Middle Devonian terrigenous rocks of the Uchulen-Kazankol complex.

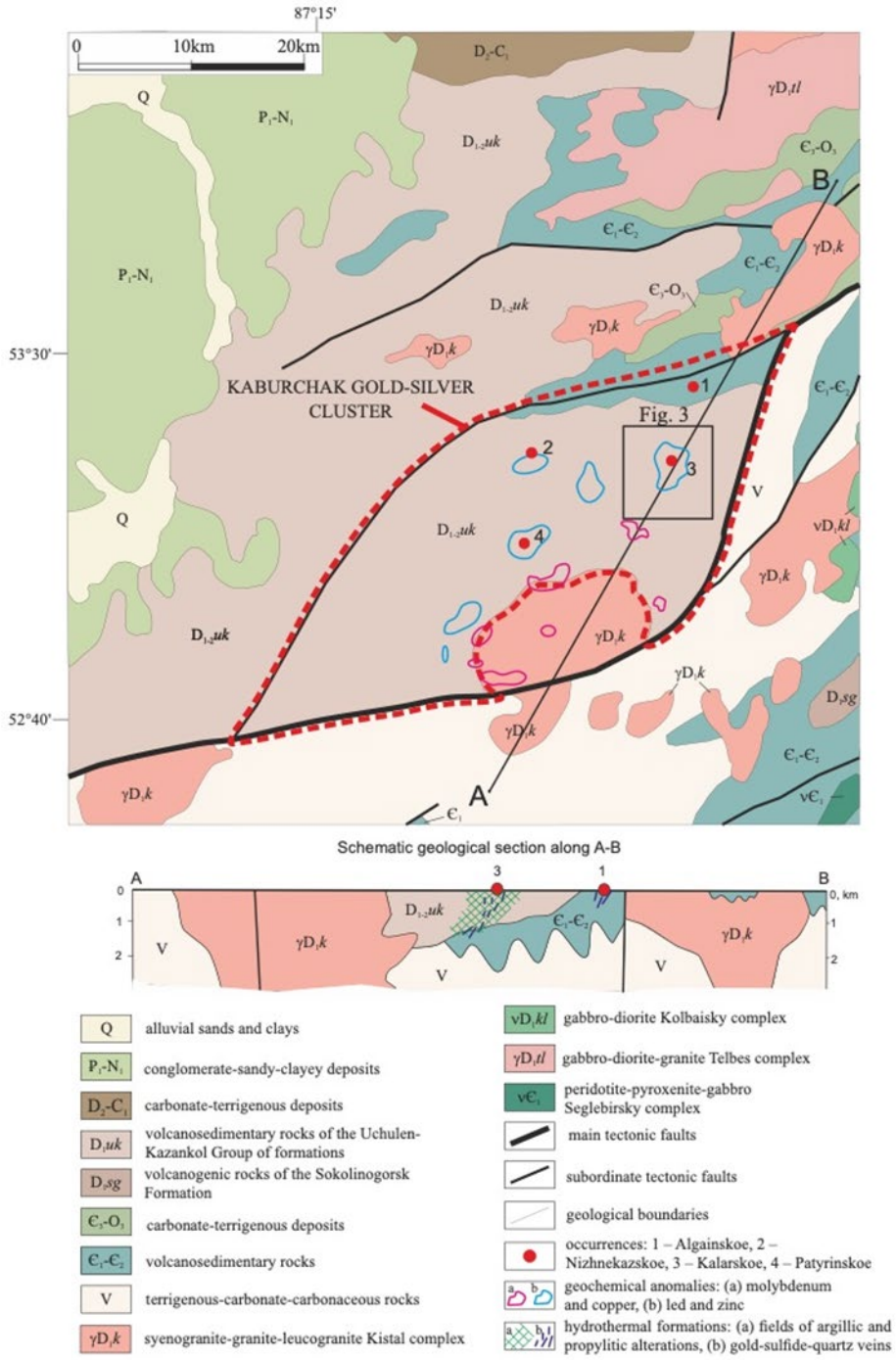


Figure 2. Schematic map showing geological features and Au-bearing potential of the Kaburchak cluster (Figure 3).

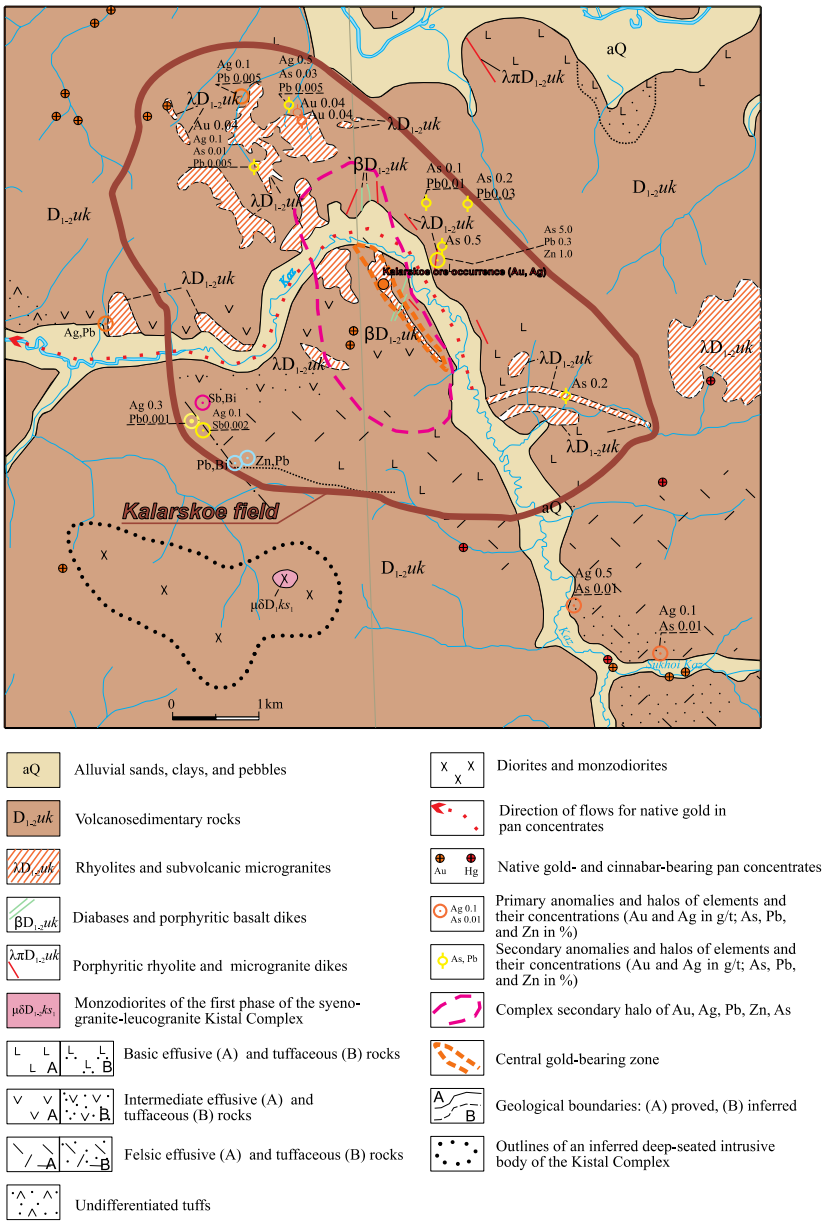
Au-Ag mineralization has been revealed at several sites within the Kaburchak cluster. These sites are characterized by the presence of (i) native Au, barite, malachite, and galena in the heavy mineral concentrates from the alluvial and diluvial deposits; (ii) Au, Ag, Pb, Zn, As, Sb, and Hg geochemical anomalies; (iii) quartz veins, sulfide mineralization, and argillic-altered zones; (iv) mineralized points with the presence of Au, Ag, and Pb (Kalarskoe, Nizhnekazskoe, Patyrinskoe, Algainskoe).

There are signs of geochemical zoning within the Kaburchak cluster. Anomalies of Mo and Cu are spatially related to the granitoids and the exocontact zones of the Kistal

massif, while geochemical anomalies of Pb and Zn are fixed at a distance within the volcano-sedimentary rocks (see Figure 2).

In 1968, intensive geological mapping in the northeastern region of the Kaburchak cluster revealed a complex geochemical anomaly characterized by elevated concentrations of Pb, Zn, and Ag in the surface sediments. Investigation of this anomaly through trenching and excavation efforts led to the identification of the Kalarskoe Au-Ag occurrence. Further exploratory studies of the Kalarskoe occurrence were conducted during the prospecting activities for Au within the Kaburchak cluster in 1977. Comprehensive exploration and research initiatives were only undertaken in the 21st century [1,2,9–11].

The Neogene and Quaternary clayey sediments with thicknesses up to 20–30 m (sometimes, up to 50 m) are widely distributed within the area and hinder the investigation of the Au-bearing potential of the Kaburchak cluster from the surface. Small-scale drilling was carried out in the northeastern segment of the Kaburchak cluster, where the Kalarskoe Au-Ag occurrence is located. The site is characterized by numerous primary and secondary geochemical anomalies of Au-accompanying elements: Ag, As, Pb, Zn, Sb, and Bi (Figure 3).



aQ — Alluvial sands, clays, and pebbles

$D_{1-2}uk$ — Volcanosedimentary rocks

$\lambda D_{1-2}uk$ — Rhyolites and subvolcanic microgranites

$\beta D_{1-2}uk$ — Diabases and porphyritic basalt dikes

$\lambda\pi D_{1-2}uk$ — Porphyritic rhyolite and microgranite dikes

$\mu\delta D_1 ks_1$ — Monzodiorites of the first phase of the syeno-granite-leucogranite Kistal Complex

A | B — Basic effusive (A) and tuffaceous (B) rocks

A | B — Intermediate effusive (A) and tuffaceous (B) rocks

A | B — Felsic effusive (A) and tuffaceous (B) rocks

Undifferentiated tuffs

Diorites and monzodiorites

Direction of flows for native gold in pan concentrates

Au | Hg — Native gold- and cinnabar-bearing pan concentrates

Ag 0.1 As 0.01 — Primary anomalies and halos of elements and their concentrations (Au and Ag in g/t; As, Pb, and Zn in %)

As, Pb — Secondary anomalies and halos of elements and their concentrations (Au and Ag in g/t; As, Pb, and Zn in %)

Complex secondary halo of Au, Ag, Pb, Zn, As

Central gold-bearing zone

A | B — Geological boundaries: (A) proved, (B) inferred

Outlines of an inferred deep-seated intrusive body of the Kistal Complex

Figure 3. Schematic geological prospecting map showing the Au-Ag Kalarskoe occurrence.

Drilling revealed that stratified rocks within the Kalarskoe field are represented by the lower sequence of the Early-Middle Devonian Uchulen-Kazankol complex, pre-dominantly by effusive rocks of intermediate and mafic composition, which are replaced by the felsic varieties in the southwest area. Within the Kalarskoe field, the shares are as follows: andesites—50%; basaltic andesites—15%; basalts—8%; andesitic tuffs—15%; mafic tuffs—11%; and tuffs of felsic and mixed composition—1%.

Eight Au-bearing zones were identified within the Kalarskoe occurrence, which are represented by intensely hydrothermally altered rocks. The Au-bearing zones are from 5 to 100 m in thickness and from 100 to 1100 m in length. The position of the Au-bearing zones and the mineralized bodies within them is controlled by faults and dikes of dacite and rhyolite composition that intersect the host rocks at different angles. The upper parts of most of the mineralized zones are oxidized. To the depth of 15–35 m, the cavernous mineralized rocks of kaolinite-sericite-scorodite-quartz-goethite composition are developed. Based on the sampling of trenches and the small amount of drilling conducted in 1970–1980 within the Au-bearing zones, with varying degrees of reliability, 28 mineralized bodies were established, with grades of Au from 0.7 g/t to 5.6 g/t and Ag from 0.2 to 570 g/t, with a prevailing thickness of about 1–2 m and lengths of up to 100 m along the strike [12].

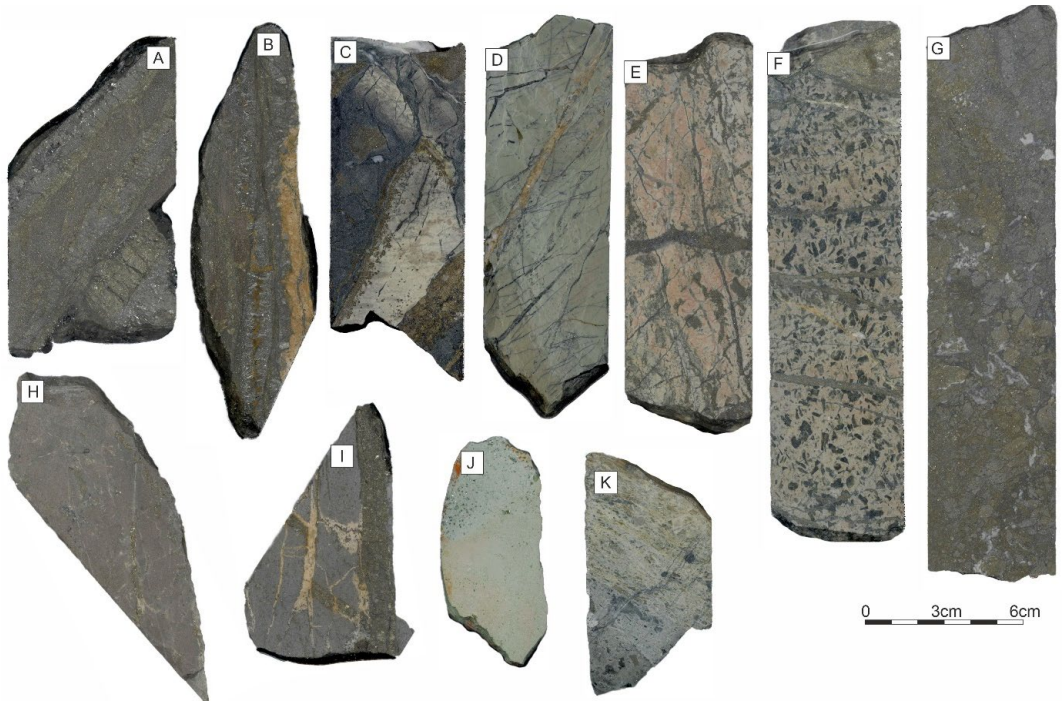
The thickest and the most studied central Au-bearing zone (Figure 3) represents a northwest-elongated zone of brecciated argillic-altered rocks confined to dikes of dacite porphyries of the Uchulen-Kazankol complex. The thickness of the zone is 50–100 m, and the established length is about 1100 m. The mineralized bodies, with a thickness of 1–7 m and a length of up to 150 m, are represented by argillic-altered rocks, with numerous quartz veinlets and veins of sulfide minerals. To the north, the zone is traced to the right bank of the Kaz River, where it is covered by alluvial and Quaternary slope clayey deposits (see Figure 3) [2].

Additional geological exploration work was carried out within the Kalarskoe field in 2018–2020, which included the drilling of 12 core wells, with a drilling depth of 100 to 210 m [10]. As result, mineral resources with an average Au content of 2.35 g/t were estimated. It is expected that further exploration of the Kalarskoe occurrence will lead to the emergence of a small Au deposit, with associated Ag.

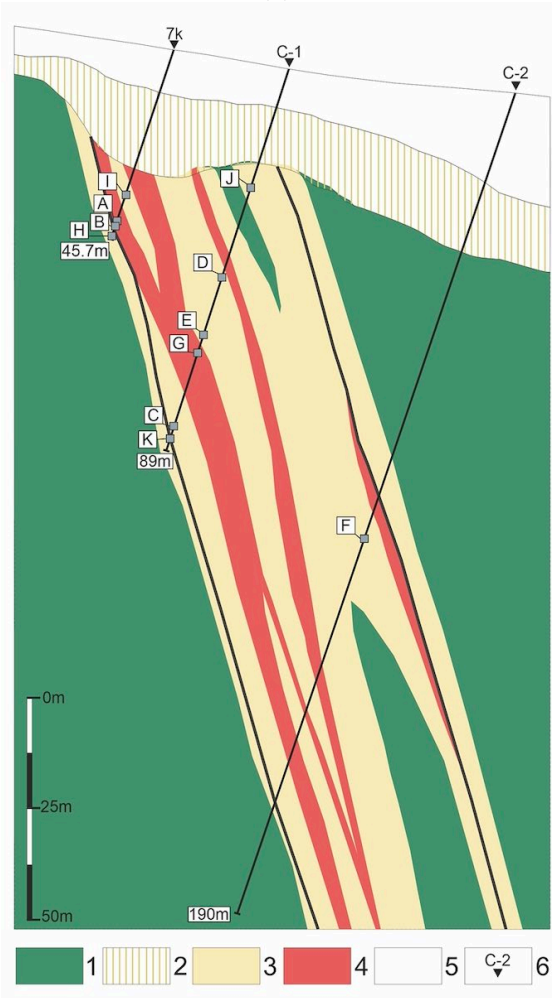
5. Mineralogical and Geochemical Features of Mineralization and Altered Rocks

Within the Kalarskoe occurrence, propylites with a relict porphyry texture are widespread and can be traced in wells to a depth of 150 m. They are characterized by the presence of (mainly) albite, chlorite, epidote, and quartz, with local rutile, pyrite, and pyrrhotite. Argillic-altered rocks with a sponge-like texture overprint the early alteration and are located near the mineralized vein selvages. According to XRD results [9], mineral assemblages of argillic alteration include quartz, illite, sericite, and chlorite, with lesser amounts of kaolin, disseminated pyrite, and rutile. The thickness of the argillic-altered zones is usually 1–10 m. They can be traced along the strike, and dip they to depths of 50–100 m; in some areas, the thickness reaches 30 m, and the zone can be traced for 500 m to a depth of up to 200 m. Photographs of metasomatite samples from drill cores of a central mineralized body are shown in Figure 4. The mineral composition and zoning of alteration are presented in Table 2.

The Au-Ag mineralization of the Kalarskoe occurrence forms a series of sulfide-quartz veins and veinlets hosted by altered brecciated volcanic and subvolcanic dacite and andesite porphyries. The gangue minerals of veins in propylites are predominantly calcite, quartz, and chalcedony, with local chalcopyrite, pyrrhotite, marcasite, and pyrite. Veins in argillic-altered rocks (up to 0.5 m in width, with a sulfide vol. % of 65–70) contain mainly pyrite and arsenopyrite, with lesser amounts of calcite, kutnohorite, quartz, rhodochrosite, sphalerite, chalcopyrite, galena, and rarely, fahlores [1,9,10].



(**a**)



(**b**)

Figure 4. (**a**) The mineral composition and zoning of altered wall rocks of the Kalarskoe occurrence, according to Ref. [9] and new data. Samples from drill holes C1, C2, 7k, and S-17; (A, B, G—massive

pyrite-arsenopyrite body; C—superimposed argillic alteration on propylite with disseminated pyrite and its veinlets; D, E, H, I—argillic metasomatites, with sulfide and later, carbonate (Ca, Mn) veinlets; F—relict porphyry texture of argillic-altered rock; J—argillic metasomatite with disseminated pyrite; K—argillic-altered rock with schistose structure. (**b**) Simplified geological cross-section of the Kalarskoe occurrence (all volcanic rocks were propylitically altered) (modified after Ref. [10]) (1) propylitic alteration; (2) hypergene zone; (3) argillic alteration with disseminated pyrite and its veinlets; (4) pyrite-arsenopyrite veins; (5) quaternary sediment; (6) number of drill holes. Letters corresponds to the sample numbers from (**a**).

Table 2. The mineral composition and zoning of altered wall rocks of the Kalarskoe occurrence, according to Ref. [9] and new data.

Mineralized Veins and Veinlets	Argillic Alteration (Rarely, Relict Porphyry Texture)		Propylitic Alteration (Local Relict Porphyry Texture)		Dacite and Andesite Porphyries
Pyrite Arsenopyrite Calcite Kutnohorite Quartz ±Rhodochrosite ±Sphalerite ±Chalcopyrite ±Galena ±Sulfosalts ±Electrum, Au	Inner	Outer	Outer	Inner	phenocrysts: plagioclase, ±pyroxene, amphibole Matrix has a felsic or intermediate content
	Quartz Illite ±Kaolinite ±Pyrite ±Rutile	Quartz Illite Chlorite ±Sericite ±Pyrite ±Rutile	Albite Chlorite Quartz ±Pyrite ±Pyrrhotite ±Rutile	Albite Chlorite Epidote Quartz ±Pyrite ±Pyrrhotite ±Rutile	

6. Methods

6.1. Material

The mineralogical and geochemical studies were conducted on mineralized samples from the seven drill holes (drilled by Rosgeologiya) within the Kalarskoe occurrence. These samples were derived from depths between 40 to 160 m, representing fragments of the central mineralized bodies. In addition, a heavy mineral concentrate was panned from the lower part of colluvium in the vicinity of the drilling sites.

6.2. Mineralogical and Geochemical Studies

From all of the collected samples (n~200), polished sections were prepared for ore microscopy. Mineralogical studies were performed using an Olympus BX 51 optical microscope (Olympus Life and Material Science Europa GmbH, Tokyo, Japan) in the laboratory of Mineralogy and Petrology, TSINIGRI. The most representative samples were additionally studied using SEM (TESCAN MIRA (TESCAN Group, Brno, Czech Republic)) with PulseTor 30 (PulseTor LLC, Pennington, NJ, USA) add-on (EDAX Element 30, EDAX Inc., Pleasanton, CA, USA)) in compatibility mode) at TSNIGRI and EPMA (JEOL JXA-8200) (JEOL, Ltd., Tokyo, Japan) at IGEM RAS. All analyses were conducted using the standard manufacturer user guide recommendations and suggestions for mineral analyses provided in Ref. [13].

The bulk concentration of the chemical elements within the metasomatic rocks were obtained for the samples derived from the C2 drill hole employing the ICP-MS Perkin Elmer Sciex Elan 610, IMGRE, (PerkinElmer Corporation, Waltham, MA, USA) using in-house standard protocol MVI No. 001-XMS-2007 (government certificate number for conformity to general requirements for the competence of testing and calibration laboratories № RA.RU.513694). Based on the results from the chemical analyses of 22 samples, an elemental correlation analysis was carried out.

6.3. (U,Th)-He Dating

The (U,Th)-He method is based on the radioactive decay of isotopes of U and Th. Recent studies of helium behavior in the crystal lattice of pyrite have shown that pyrite exhibits a high preservation of helium and can be used as a (U,Th)-He geochronometer [14–16].

For (U,Th)-He dating, pyrite grains with sizes > 200 µm were manually extracted from two optically studied mineralized rock fragments (Figure 5; drill hole 7k; sampling depths 33.3 and 40.1 m). For (U,Th)-He dating, pyrite grains from each of the samples were divided into several subsamples consisting of from 1 to 4 pyrite grains with a joint weight of 1.5–2 mg.

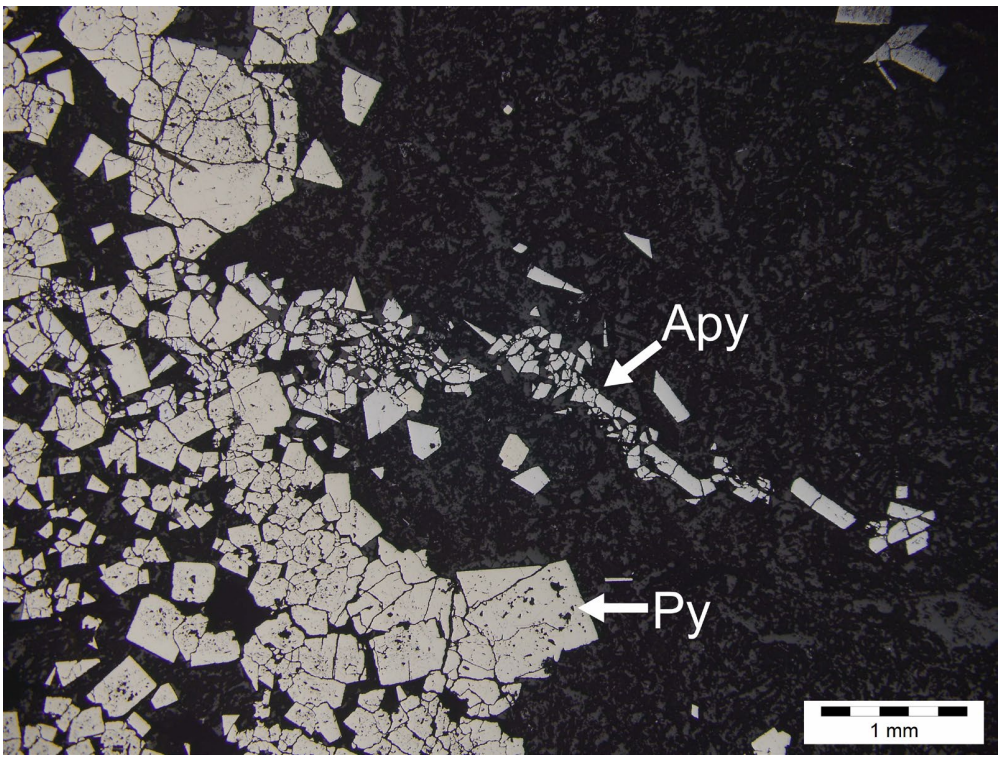


Figure 5. Photomicrograph of a massive pyrite-arsonopyrite assemblage at a 33.3 m depth from drill hole 7k. Some of the pyrite grains in this sample were used for (U-Th)-He dating. Py—pyrite; Apy—arsenopyrite.

The content of radiogenic ^{4}He in the pyrite grains was measured with a high-sensitivity magnetic sector mass spectrometer, MSU-G-01-M (Spectron Analyt, St. Petersburg, Russia), at IPGG RAS [17]. The pyrite grains were placed in a quartz ampoule and sealed after obtaining a vacuum condition (10^{-3} torr) in order to prevent U and Th loss during He extraction [15]. A sealed quartz ampoule was placed in the high vacuum furnace of the mass spectrometer. During measurement, the samples were heated in several steps to 1100 °C, according to the protocol described in Ref. [16]. The quartz ampoule of the degassed samples was spiked with a ^{230}Th-^{235}U tracer and dissolved in a mixture of concentrated hydrofluoric acid (0.5 mL), nitric acid (0.1 mL), and perchloric acid (0.05 mL) in closed Teflon vials for 48 h in an autoclave at a temperature of 220 °C. The isotope ratios of U and Th were measured on the ELEMENT XR ICP mass-spectrometer (Thermo Fisher Scientific, Waltham, MA, USA) at the GEOKHI RAS. Empty quartz ampoules were used to determine the representative blank of the He, U, and Th measurements. The accuracy of the complete dating procedure was assessed using simultaneous experiments on a Durango apatite, which is the international standard for the (U,Th)-He method. (U,Th)-He ages were calculated using IsoplotR software ver. 6.2.1 [18]. Alpha-recoil corrections were not applied, as the grains were extracted from the massive pyrite allocations.

7. Results

7.1. Mineralogical and Geochemical Observations

Based on the results of the ICP-MS analysis of the mineralized rocks and metasomatites, it was found that Au has a positive correlation with such elements as As (0.84), Te (0.83), Sb (0.69), Pb (0.63), and Ag (0.66), with a critical value of ±0.54. The variation in the element concentrations with the depth of the C2 drill hole is presented in Figure 6; the full chemical data are available in the Supplementary Material File S1. The maximum Au content, which reached up to 1.4 ppm, was obtained for the samples with depths of 84 and 140 m.

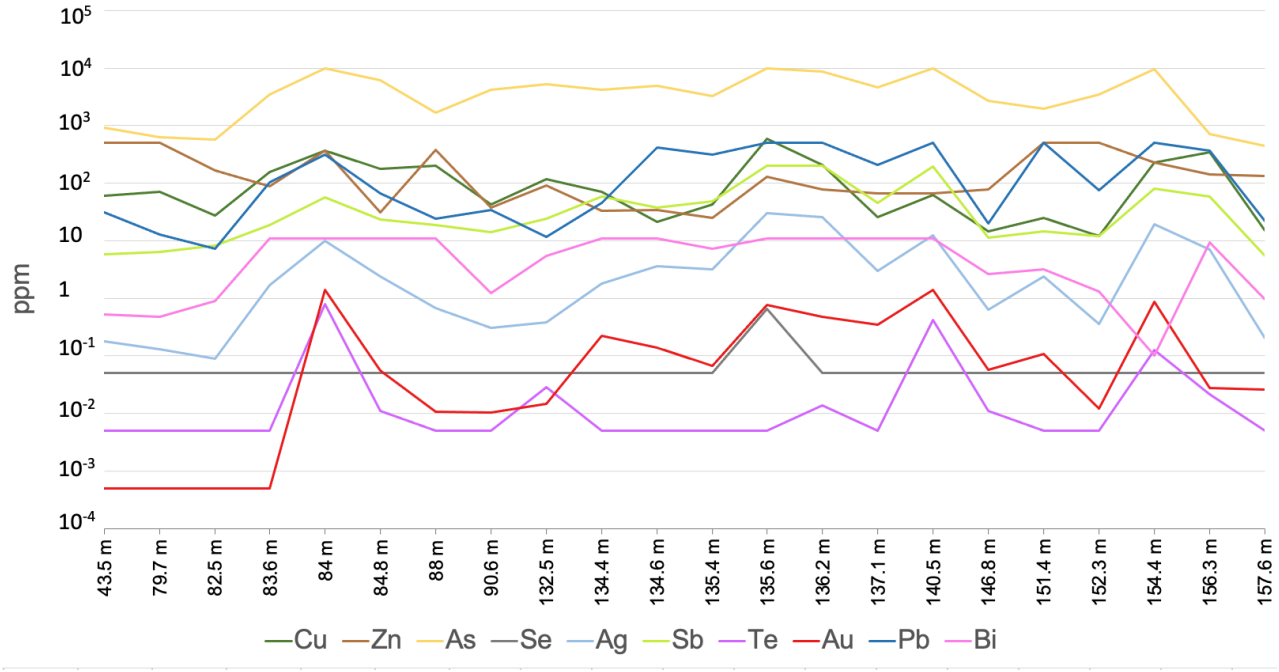


Figure 6. Changes in the content of elements with depth in the mineralized rocks and metasomatites from drill hole C2, based on the results of ICP-MS analysis. The vertical axis is the content of elements (ppm) on the logarithmic scale. The horizontal axis is the sampling depth.

Among the ore minerals within the Kalarskoe occurrence, the most widespread are pyrite and arsenopyrite, with lesser amounts of pyrrhotite, chalcopyrite, galena, and sphalerite, and rare occurrences of fahlores, sulfosalts, electrum and native Au.

The study of the mineralogical composition of the samples made it possible to detail and supplement previously performed studies [9]. Pyrite occurs as a product of pyrrhotite replacement in propylites (pyrite-1), as scattered idiomorphic crystals in argillic metasomatites (pyrite-2), as veinlets in metasomatites (pyrite-3), and as massive veins intergrown with arsenopyrite (pyrite-4). Pyrite-1, in association with marcasite, forms fine-crystalline pseudomorphs with pyrrhotite-1 (Figure 7D), often with the formation of a "bird's eye" texture. Pyrite-2 (Figure 7A) is characterized by a sieve texture formed due to inclusions of sericite/illite, quartz, and leucoxene, with a lattice texture (pseudomorphs in association with ilmenite in magnetite). Pyrite-3 forms euhedral crystals that compose veinlets and vein selvages. It is worth noting that there are almost no inclusions in pyrite-3 (Figure 7B). Pyrite-4 (Figure 7C) forms massive crystalline aggregates along with arsenopyrite-2, which is fragmented by subsequent processes.

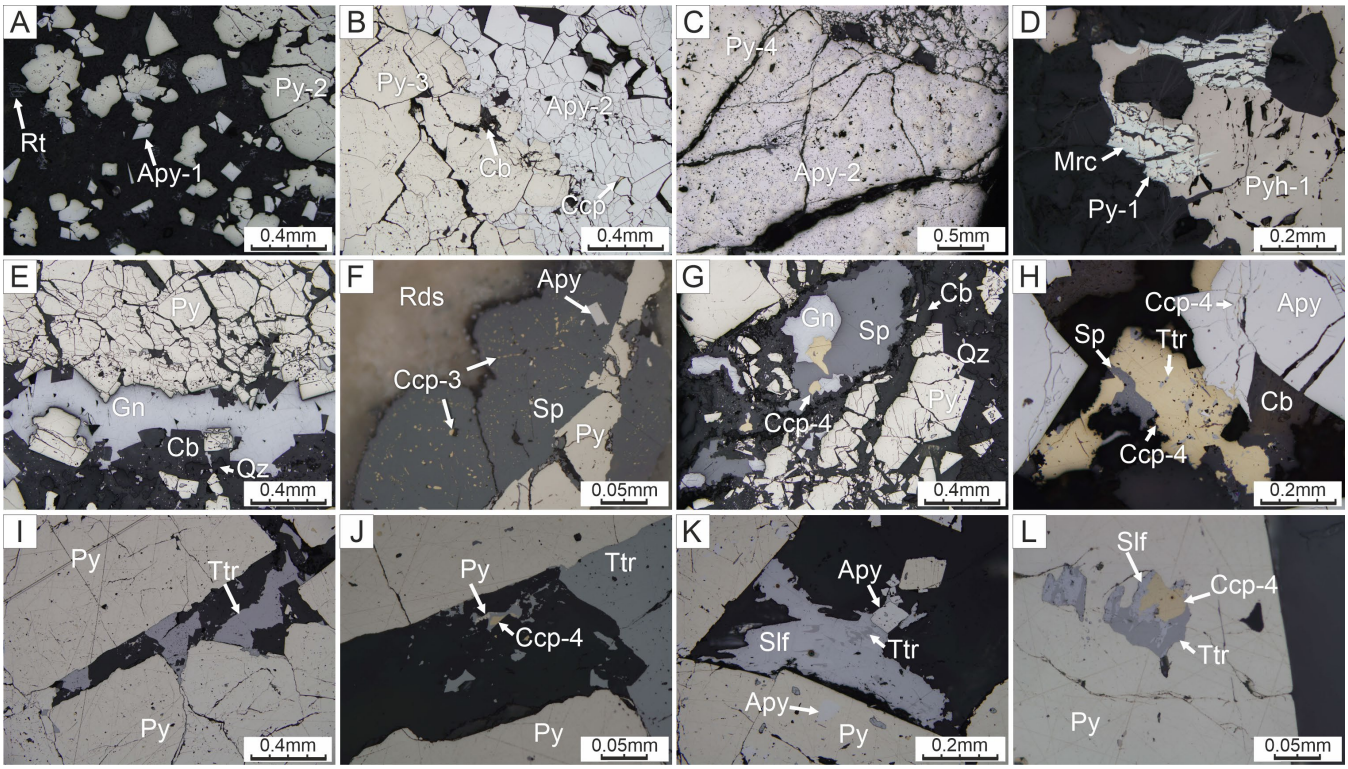


Figure 7. Images of polished sections (updated based on the work of Leibham, 2022 [9]). (**A**)—disseminated pyrite and arsenopyrite in the argillic-altered rock; (**B**,**C**)—massive pyrite-arsenopyrite vein; (**D**)—pyrrhotite and chalcopyrite in the propylite; (**E**)—pyrite vein crossed by galena-carbonate veinlet; (**F**)—pyrite and arsenopyrite fragments in sphalerite with inclusions of chalcopyrite; (**G**)—sphalerite, galena, and chalcopyrite in the carbonate veinlet; (**H**)—later chalcopyrite with fahlore; (**I**,**J**)—fahlore in the carbonate veinlet; (**K**)—sulfosalt with relicts of fahlore; (**L**)—the intergrowth of fahlore, chalcopyrite, and sulfosalt. Apy—arsenopyrite; Cb—carbonates; Ccp—chalcopyrite; Gn—galena; Py—pyrite; Pyh—pyrrhotite; Qz—quartz; Rds—rhodochrosite; Rt—rutile; Slf—sulfosalts; Sp—sphalerite; Ttr—tetrahedrite.

Arsenopyrite occurs as disseminated euhedral crystals in argillic-altered rocks near vein selvages and often contains inclusions of pyrite-2 and pyrrhotite-2 (arsenopyrite-1, Figure 7A). In addition, the mineral was observed in massive veins intergrown with pyrite, as veinlets cutting earlier formed pyrite-3 (arsenopyrite-2; Figure 7B,C), and as small euhedral crystals in the carbonate.

Pyrrhotite occurs as disseminated allotriomorphic crystals in propylites (pyrrhotite-1; Figure 7D) and also as irregularly shaped inclusions in arsenopyrite-1 (pyrrhotite-2).

Chalcopyrite is characterized by allotriomorphic crystals. It is noted in intergrowths with pyrrhotite-1 (chalcopyrite-1) and rarely, with pyrrhotite-2 (chalcopyrite-2). Furthermore, it was found in the form of inclusions n sphalerite (chalcopyrite-3; Figure 7F) and later overgrowth along the rim and veinlets (chalcopyrite-4; Figure 7H). Chalcopyrite-4 often cements small fragments of arsenopyrite (Figure 7H) and fills intercrystalline spaces in it and in pyrite. The mineral also overgrows fahlore (chalcopyrite-4; Figure 7J,L).

Galena forms irregularly shaped crystals in carbonate veins and veinlets and in fractured pyrite with sulfosalts (Figure 7E,G).

Fahlore is noted mainly in carbonate veinlets and in fractures or voids in pyrite (Figure 7I,L).

Sulfosalts are located at the interstices between pyrite and arsenopyrite, as well as along fractures in intergrowths of pyrite and arsenopyrite. In the largest crystal intergrowths, relics of fahlore are noted; relics of chalcopyrite are less common (Figure 7K,L).

Sphalerite is characterized by an average iron content of 2.5 to 10.2% (Table 3) and a small constant admixture of Cd (0.3–0.6 wt.%).

Fahlores, according to previous studies, are represented by tetrahedrite-(Zn) [9] (Figure 8). New data indicate the presence of tetrahedrite (Fe) in the ores, which is also characterized by a constant small admixture of Ag (Table 4).

The general formula of fahlores, according to the EPMA results, is shown below, based on 29 atoms in the formula:

$$(Cu_{8.74-9.95}, Ag_{0.29-0.40})_{\Sigma = 9.13-10.27}\ (Zn_{0.75-1.06}, Fe_{0.84-1.76}, Pb_{0-0.11})_{\Sigma = 1.84-2.53}$$
$$(Sb_{3.95-4.29}, As_{0.01-0.09}, Bi_{0.01-0.14})_{\Sigma = 4-4.30}\ S_{12.45-13.48}$$

The general formula of fahlores, according to the SEM results, based on 29 atoms in the formula:

$$(Cu_{9.4}, Ag_{0.1})_{\Sigma = 9.5}\ (Zn_{1.2}, Fe_{1.6})_{\Sigma = 2.8}\ Sb_{3.9}\ S_{12.9}$$

Table 3. Chemical composition of sphalerite (wt.%) according to the results of EPMA (1–2) and SEM (3–9).

n	Ag	Cu	Hg	Zn	Fe	Cd	In	Mn	S	Total
1	0.01	0.59	0.03	62.99	3.22	0.62	0.04	0.03	33.41	100.93
2	0.00	0.75	0.02	62.36	3.59	0.54	0.06	0.03	33.51	100.86
3				54.7	10.2	0.6			33.7	99.1
4				60.3	5.5	0.4		0.4	33.5	100.1
5				56.4	9.2	0.5			34.1	100.2
6				58.4	7.4	0.4			33.7	99.9
7				59.5	7.2	0.5			32.8	100.0
8				62.4	2.5				35.1	100.0

Notes: *n* is hereinafter used as the analysis number.

Table 4. Chemical composition of fahlores (wt.%) from the results of EPMA (1–13) and SEM (16).

n	Sb	Se	S	Cu	Ag	As	Bi	Zn	Pb	Fe	Hg	Total	Tetrahedrite Type
1	29.37		25.12	35.18	2.16	0.08	0.19	4.09	0.05	2.89		99.12	Zn
2	28.74		24.88	33.88	2.00	0.13	1.74	4.04	1.33	2.73		99.46	Zn
3	29.68	0.03	25.04	34.77	2.54	0.10	0.43	3.72	0.12	3.17		99.60	Zn
4	28.46	0.02	24.85	34.39	2.52	0.09	0.93	3.37	0.78	4.29		99.69	Fe
5	29.41	0.01	25.37	34.03	2.61	0.09	0.23	3.11	0.16	5.36	0.03	100.42	Fe
6	29.07	0.02	25.81	33.55	2.50	0.09	0.37	2.98	0.16	5.94	0.02	100.51	Fe
7	29.22	0.01	25.27	35.75	2.16	0.15	0.15	3.72	0.06	3.69		100.18	Fe
8	29.43		25.18	35.63	1.94	0.13	0.19	3.85	0.09	3.41		99.85	Fe
9	29.15		25.47	36.85	1.91	0.12	0.11	4.05	0.02	3.15		100.83	Zn
10	30.16		23.05	36.54	1.96	0.02	0.11	3.52	0.03	3.39		98.78	Fe
11	30.24	0.01	25.08	33.49	2.28	0.04	0.10	3.39	0.05	3.19	0.06	97.92	Fe
12	30.20		25.12	33.27	2.42	0.04	0.07	3.32	0.08	3.10		97.60	Fe
13	29.41		25.32	35.47	2.07	0.39	0.19	3.54	0.07	3.61		100.07	Zn
16	28.3		24.5	35.6	0.7			4.5		5.2		98.8	Fe

Notes: *n* is hereinafter used as the analysis number.

According to the data obtained, sulfosalts are comprised of jamesonite and bournonite (Figure 8). The composition of jamesonite is shown in Tables 5 and 6. Jamesonite was calculated for 10 cations, excluding Cu and Fe, based on the jamesonite formula $FePb_4Sb_6S_{14}$ [19]. The impurity of Ag was taken into account in the formula considering the units of Pb similar to the data given in Ref. [20], and the calculation for 25 atoms was also performed (Table 6). The increased iron content can be explained by the location of small jamesonite secretions in pyrite and the capture of iron from it.

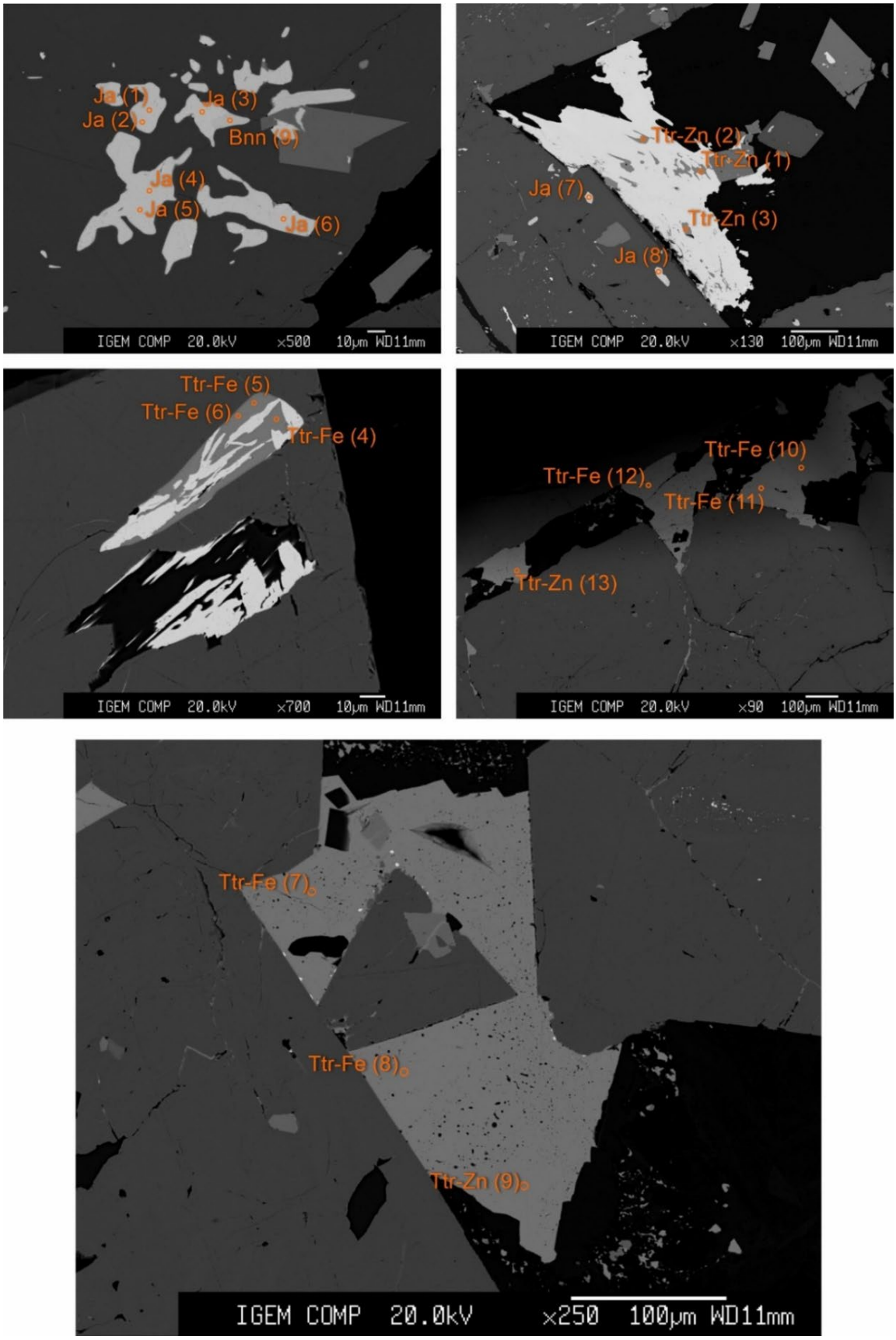


Figure 8. BSE images of jamesonite (Ja), bournonite (Bnn), tetrahedrite-(Fe) (Ttr-Fe), and tetrahedrite-(Zn) (Ttr-Zn). The numbers of the analyses are shown in parentheses.

Table 5. Chemical composition of jamesonites (wt.%), according to the results of EPMA.

n	Sb	Se	S	Cu	Ag	As	Bi	Zn	Pb	Fe	Te	Hg	Total
1	29.86	0.03	21.36	0.04	0.07	0.03	8.04		37.36	3.40			100.19
2	29.08	0.06	21.31	0.02	0.12	0.03	7.99		37.50	2.95			99.06
3	29.10		21.35	0.09	0.15	0.06	8.24		37.23	3.57			99.79
4	29.95		21.27	0.04	0.04	0.05	7.91	0.04	37.91	3.06			100.25
5	29.51	0.02	21.28	0.03		0.06	8.04		37.74	2.84		0.04	99.56
6	28.73	0.01	21.13	0.08		0.05	9.01		37.43	3.30			99.75
7	30.05		20.83	0.04		0.07	7.38		37.61	3.75	0.01		99.73
8	25.68		20.19	0.04			13.77		36.91	3.53			100.11

Notes: *n* is hereinafter used as the analysis number.

Table 6. Formula units of jamesonites.

Formula Units Based on (Pb + Ag + Sb + Bi + As) = 10															
n	Sb	Se	S	Cu	Ag	As	Bi	Zn	Pb	Fe	Cu + Fe + Zn	Bi + Sb + As	Bi/Sb	(Pb + Ag)/(Sb + Bi)	S + Se + Te
1	5.27	0.01	14.32	0.01	0.01	0.01	0.83		3.88	1.31	1.32	6.11	0.16	0.64	14.33
2	5.20	0.02	14.46	0.01	0.02	0.01	0.83		3.94	1.15	1.16	6.04	0.16	0.66	14.48
3	5.19		14.47	0.03	0.03	0.02	0.86		3.90	1.39	1.42	6.07	0.16	0.65	14.47
4	5.26		14.19	0.01	0.01	0.01	0.81	0.01	3.91	1.17	1.20	6.08	0.15	0.64	14.19
5	5.22	0.01	14.31	0.01		0.02	0.83		3.93	1.10	1.11	6.07	0.16	0.65	14.31
6	5.13		14.32	0.03		0.01	0.94		3.92	1.28	1.31	6.08	0.18	0.65	14.32
7	5.31		13.99	0.01		0.02	0.76		3.91	1.45	1.46	6.09	0.14	0.64	13.99
8	4.64		13.84	0.01			1.45		3.91	1.39	1.40	6.09	0.31	0.64	13.84
Formula units based on 25 atoms															
1	5.14	0.01	13.96	0.01	0.01	0.01	0.81	0.00	3.78	1.28	1.29	5.95	0.16	0.64	13.97
2	5.07	0.02	14.10	0.01	0.02	0.01	0.81	0.00	3.84	1.12	1.13	5.89	0.16	0.66	14.12
3	5.01	0.00	13.97	0.03	0.03	0.02	0.83	0.00	3.77	1.34	1.37	5.86	0.16	0.65	13.97
4	5.18	0.00	13.97	0.01	0.01	0.01	0.80	0.01	3.85	1.15	1.18	5.99	0.15	0.64	13.97
5	5.14	0.01	14.07	0.01	0.00	0.02	0.82	0.00	3.86	1.08	1.09	5.97	0.16	0.65	14.08
6	5.00	0.00	13.97	0.03	0.00	0.01	0.91	0.00	3.83	1.25	1.28	5.93	0.18	0.65	13.97
7	5.22	0.00	13.74	0.01	0.00	0.02	0.75	0.00	3.84	1.42	1.43	5.98	0.14	0.64	13.75
8	4.59	0.00	13.71	0.01	0.00	0.00	1.43	0.00	3.88	1.38	1.39	6.03	0.31	0.64	13.71

Notes: For analysis numbers, see Figure 8. *n* is hereinafter used as the analysis number.

Bournonite was calculated for only six atoms using one analysis (Table 7, Figure 7), and the resulting formula is $(Cu_{0.95}, Fe_{0.1})_{\Sigma = 1.05}$ $Pb_{0.95}$ $(Sb_{0.97}, Bi_{0.02})_{\Sigma = 0.99}$ $S_{3.01}$. This turned out to be very close to the ideal formula of $PbCuSbS_3$.

Table 7. Chemical composition of bournonite (wt.%), according to the results of EPMA.

n	Sb	Se	S	Cu	As	Bi	Zn	Pb	Fe	Hg	Total
9	24.44	0.02	19.92	12.49	0.06	0.65	0.04	40.48	1.17	0.04	99.32

Notes: *n* is hereinafter used as the analysis number.

SEM analyses established the presence of electrum and native Au in the pyrite and arsenopyrite of the Kalarskoe occurrence (Figure 9). In electrum, the Au content varies from 34.9 wt.% up to 59.1 wt.%, and Ag ranges from 65.1 wt.% up to 40.9 wt.%, respectively. The fineness of native Au varies from 936‰ to 944‰ and from 866‰ to 885‰, respectively.

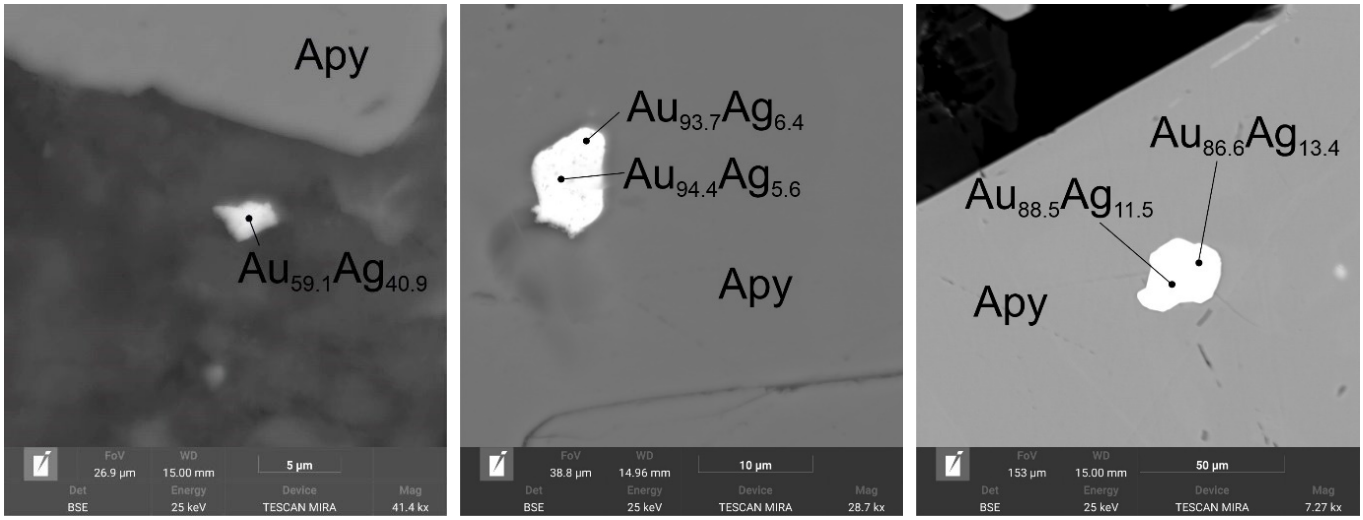


Figure 9. BSE images. The compositions of electrum and native Au at the analysis points are indicated (wt.%).

A general image of the polished section was also obtained using SEM, which shows that native Au and electrum are located in an area of brecciation of pyrite and arsenopyrite, cemented by other sulfide minerals and carbonate (Figure 10).

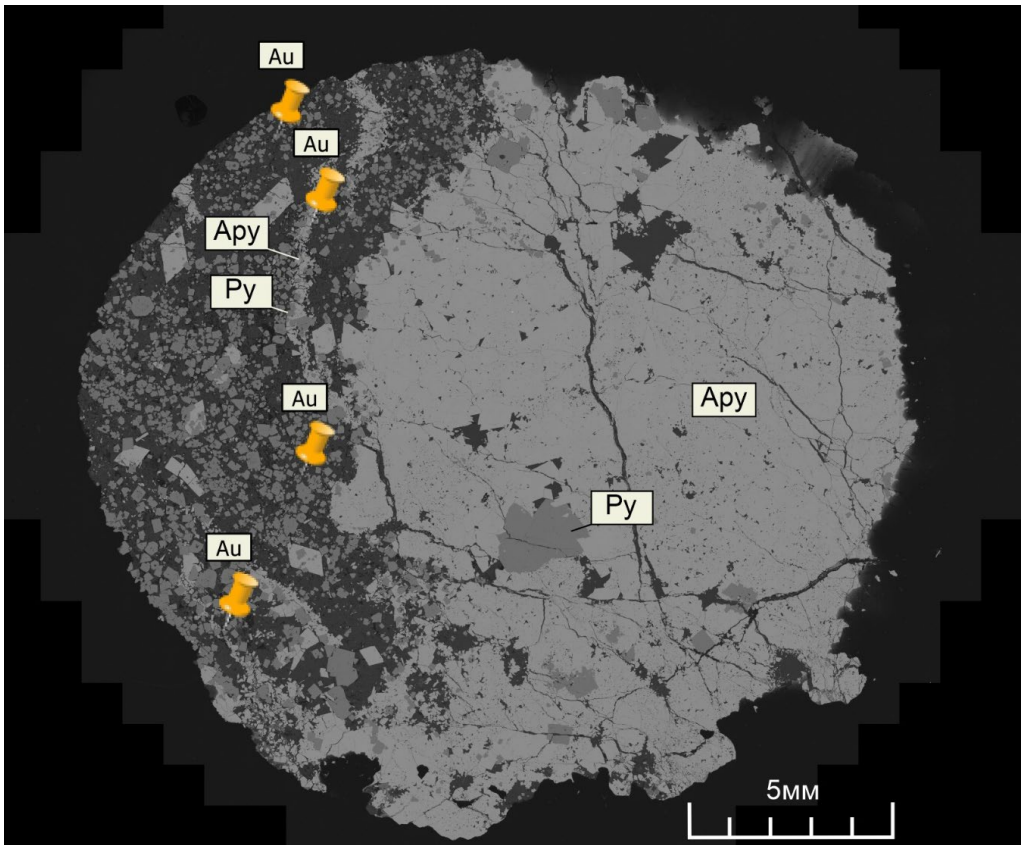
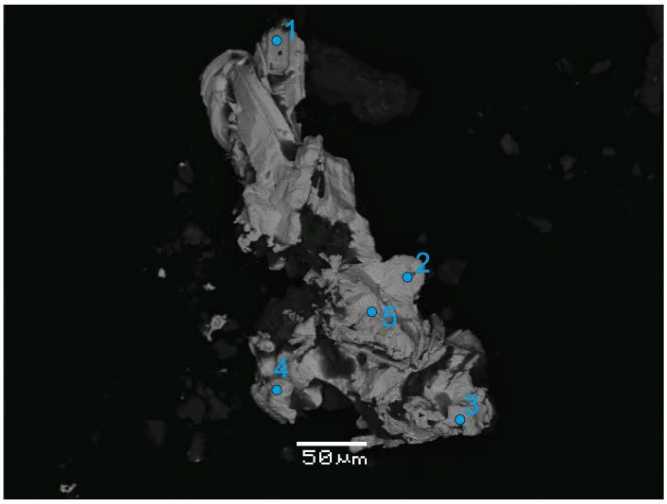
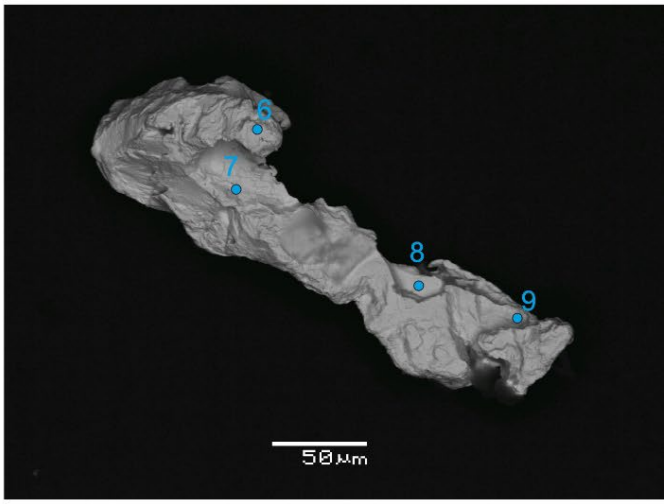


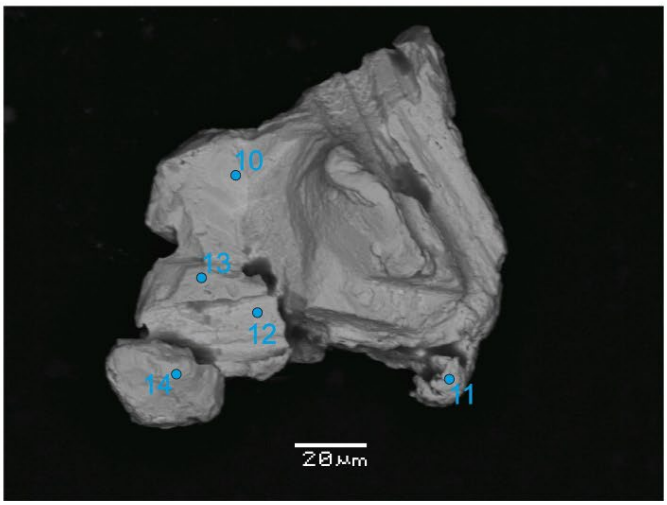
Figure 10. BSE image. A fractured pyrite-arsenopyrite aggregate with a marginal destruction zone, within which Au occurrences are noted (orange pins).

In samples of oxidized zones from the central Au-bearing zone of the Kalarskoe occurrence, thin Au (less than 0.07 mm) was found in intergrowths with quartz and sulfides. More than 30% of Au is less than 0.004 mm in size and occurs in pyrite, limonite,

arsenopyrite, scorodite, and sphalerite. According to X-ray spectral analysis, its fineness is 880‰–916‰ [1]. We studied Au from schlich samples taken from the lower part of the colluvium above the C2 well in the central zone. Au grains up to 0.4 mm in size are intergrown with transparent quartz and rarely, with limonite. Studies have shown that its fineness varies widely from 777‰ to 990‰, with predominant values at the level of 770‰–840‰ and 880‰–900‰ (Figure 11).







N	Cu	Zn	Ag	Au	Sum
1	1.18		17.04	81.78	100
2			19.77	80.23	100
3	0.79		20.9	78.31	100
4	10.7	10.57		78.74	100
5			19.62	80.38	100
6	0.72		9.73	89.55	100
7			10.06	89.94	100
8			11.36	88.64	100
9			13.35	86.65	100
10			22.28	77.72	100
11	0.99			99.01	100
12			16.44	83.56	100
13			23.26	76.74	100
14	1.1		15.66	83.24	100

Figure 11. Morphology of Au from eluvial sediments above the central Au-bearing zone of the Kalarskoe occurrence, with geochemical composition data.

7.2. Stages of the Mineralization

The mineral composition; the identification of several generations of pyrite, arsenopyrite, and chalcopyrite; variations in the chemical composition of Au; brecciation; and the crushing of mineralized bodies indicate the complicated evolution of the mineralization-forming system within the Kalarskoe field. Analysis of these complex geological, geochemical, and mineralogical data made it possible to identify several stages of the formation of hydrothermal-metasomatic rocks (Figure 12):

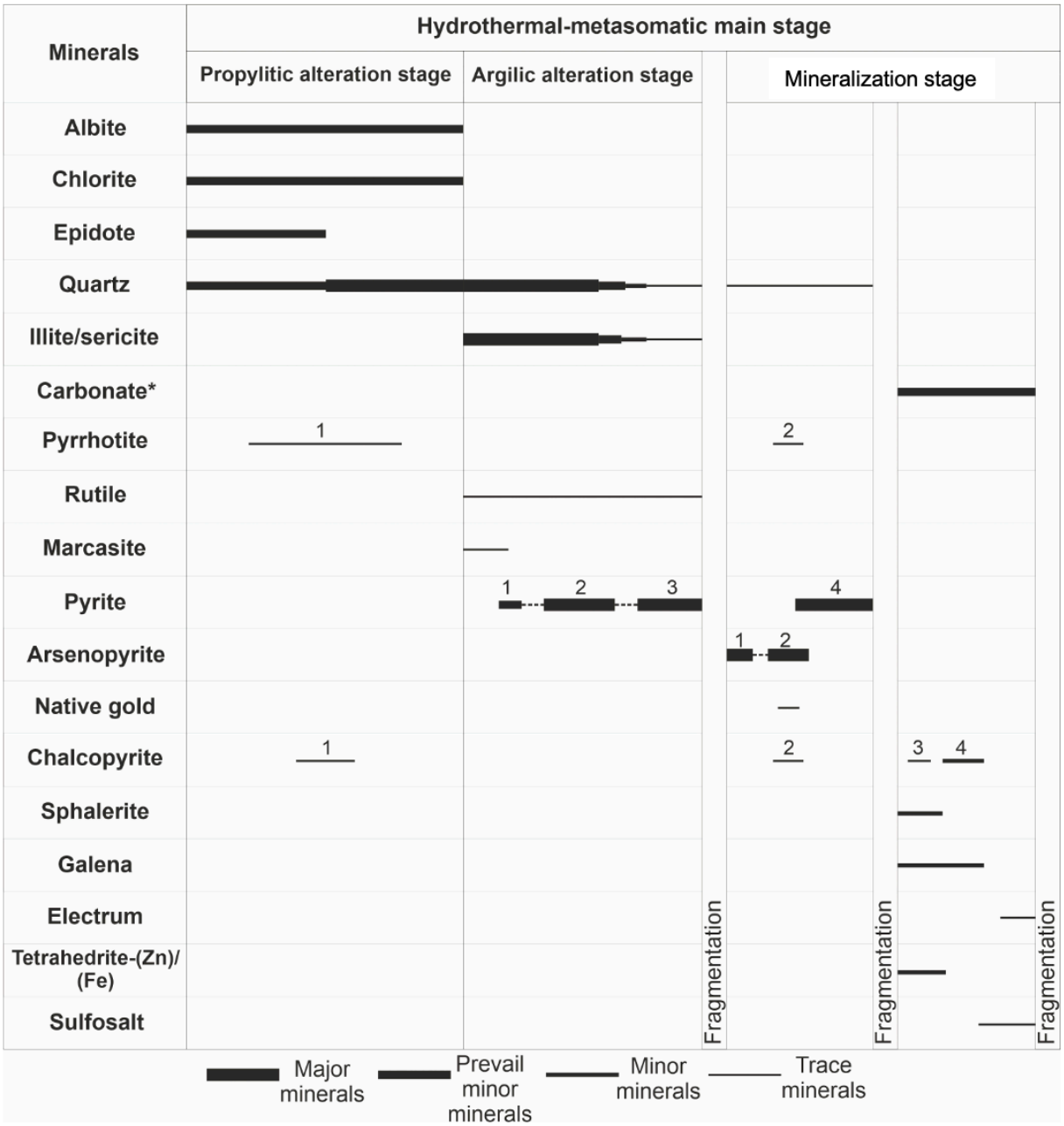


Figure 12. Paragenetic sequence of alteration and mineralization at the Kalarskoe occurrence. The numbers on the scheme indicate the different morphological forms of the minerals (see text). * calcite, kutnohorite, and rhodochrosite were identified and grouped.

Propylitic alteration in volcanic rocks: at this stage, volcanic and subvolcanic bodies of mafic, intermediate, and felsic compositions were altered by near-neutral solutions, with the formation of albite-epidote-chlorite association-1, which progressed into a lower temperature quartz-chlorite-albite association-2 (see Table 2).

Argillic alteration of volcanic and earlier-formed metasomatic rocks: during the process, propylites were overprinted into quartz-illite-chlorite rocks (outer zone) and quartz-illite rocks (inner zone) due to the presence of disseminated pyrite and its veinlets.

The hydrothermal stage (mineralization stage): at this stage, the previously formed metasomatites were brecciated and cemented by the newly formed minerals—early arsenopyrite, pyrite, and native Au, and later, by chalcopyrite, sphalerite, galena, fahlores, electrum, and sulfosalts. Early quartz and late carbonate veins and veinlets, with sulfide

minerals cutting through previously formed metasomatites, are widespread. Based on the specificity of the relationship between minerals and the structural and textural features of the mineralized bodies, it is assumed that the formation of the vein mineralization of the hydrothermal stage occurred in several pulses.

7.3. (U,Th)-He Dating Results

The (U,Th)-He ages for seven subsamples of pyrite from two distinct mineralized rock fragments within the Kalarskoe occurence were obtained (Table 8). The signals of He, U, and Th were markedly above the background level (empty quartz ampoule). The concentrations of U in the pyrite vary from 0.6–0.8 ppm, with Th/U ratios of 2.3–2.9. Concentrations of ^{4}He range from 3.2–6.4 $\times$ 10^{-5} cm^3 STP g^{-1}. The fraction of low temperature He that is released from the pyrite at temperatures below 400 °C varies from 1.5% to 2.8%.

Table 8. Results of the (U,Th)-He dating of pyrite from the Kalarskoe occurrence.

Sample	Weight, mg	He, 10^{10} at	1σ, %	U, 10^{10} at	1σ, %	Th, 10^{10} at	1σ, %	Age, Ma	±	U, ppm	Th/U	$f_{low}T$
7k-33.3 m												
1175	2.1	359	0.5	422	4.2	1117	4.5	401	20	0.8	2.7	1.6
1176	2.1	320	0.5	363	3.1	1040	2.4	402	15	0.69	2.9	2.7
1177	1.7	261	0.5	336	3.3	969	4.3	355	14	0.78	2.9	2.5
1204 *	1.7	147	1.2	156	1.4	462	1.1	425	14	0.36	3.0	1.0
1206	1.9	273	1.3	341	1.7	950	1.4	370	12	0.71	2.8	1.5
Weighted mean								377	22			
7k-40.1 m												
1089	1.1	170	0.6	225	4.0	521	2.7	373	20	0.81	2.3	2.8
1094	2.3	270	0.7	343	1.5	915	1.5	370	8	0.59	2.7	1.7
Weighted mean								371	8			
Empty quartz ampoule												
	28–56	1.1	37	1.3	97	6	74					

* Note. Sample 1204 showed a remarkably lower U content and a geologically unmeaningful age; thus, it was considered as erroneous and was not taken into account for age estimations. The reported uncertainties of the U, Th, and He measurements are the combined uncertainties calculated by summation in the quadrature of measurement and the blank uncertainties using a coverage factor of 1, which gives a level of confidence of approximately 65%.

Ages for pyrite from the Kalarskoe occurrence reveal overdispersion in a broad range from 355 to 402 Ma (Figure 13). Analysis of the possible causes of the open behavior of the (U,Th)-He system, such as interaction with groundwater, He capture during crystal growth, and thermal loss, indicate that these factors are unlikely to affect the (U,Th)-He ages of pyrite (Supplementary Material File S2). Mineral inclusions, deformations, and the presence of several generations of pyrite are more likely to result in the overdispersion of the obtained age values.

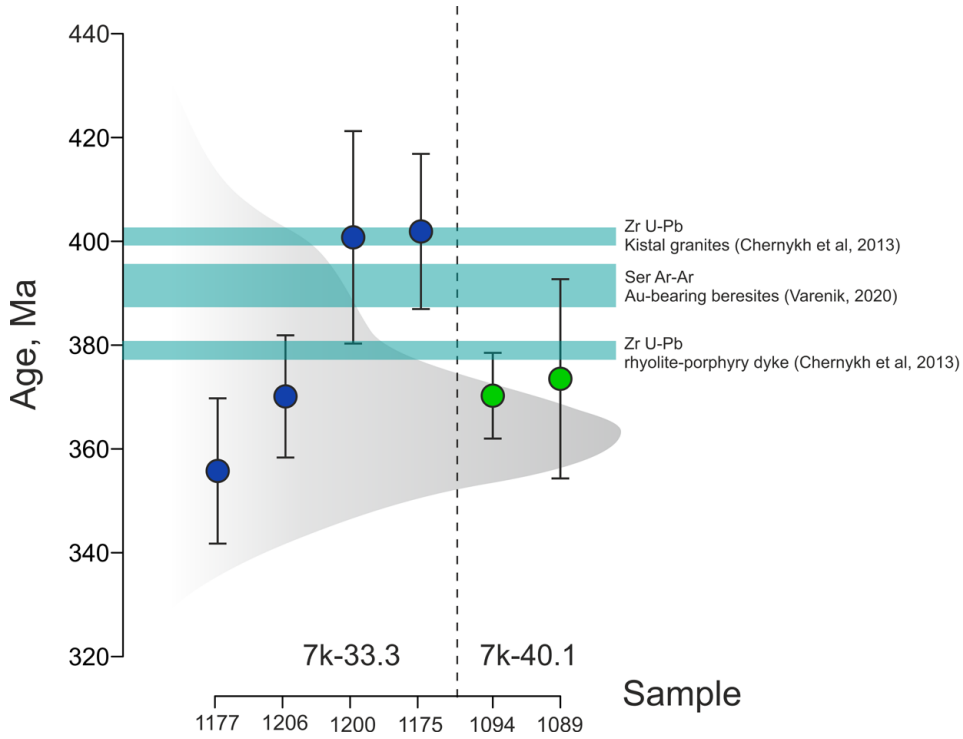


Figure 13. Distribution of (U,Th)-He ages of pyrite from the massive pyrite-arsenopyrite body, probability density plot (grey), and previous age estimations of the various rocks within the Kalarskoe field. Blue dots corresponds to the age of pyrite from the sample 7k-33.3; green dots—sample 7k-40.1. The plot is constructed using DensityPlotter software ver. 8.5 [21]. Error bars represents 2σ.

Pyrite crystallizes and recrystallizes during metamorphic, tectonic, and metasomatic events [22,23]. Mineralogical observations revealed that there are several generations of pyrite within the massive pyrite-arsenopyrite bodies, which are considered as pyrite-3 and pyrite-4 (Figure 14).

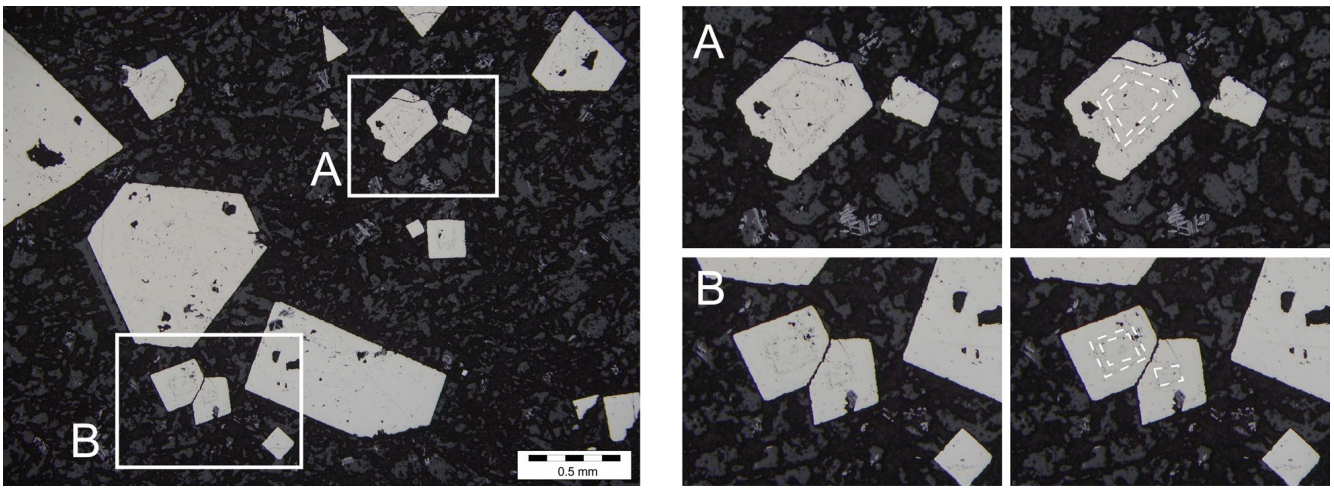


Figure 14. Images of the pyrite from the sample 7k-33.3 m, which shows at least two coexisting generations of pyrite: grains with zonation (**A**,**B**) and grains without signs of the zonation. Dotted lines are used to emphasizes the internal zoning.

Statistical analysis of the (U,Th)-He age values reveals a non-Gaussian distribution (Figure 13). Two age peaks are observed: 399 ± 18 Ma and 371 ± 7 Ma. Given the small number of grains and the absence of mineralogical control of the analyzed grains prior to

the (U,Th)-He dating, the interpretation of these age clusters is speculative. Thus, we will not specify two distinct events and will consider that the (U,Th)-He age of pyrite from the massive pyrite-arsenopyrite mineralized bodies of the Kalarskoe occurrence is in a range from ~399 to 371 Ma.

8. Discussion

8.1. Classification of the Kalarskoe Occurrence

The mineralization of the Kalarskoe occurrence exhibits a complex mineral composition. Among the major sulfide minerals are pyrite, arsenopyrite, chalcopyrite, sphalerite, galena, and pyrrhotite. The minor ore minerals include fahlores, sulfosalts, and native Au. In addition, the minerals of Ag, Bi, and Te are quite consistently present in minor amounts. In total, based on previously published Refs. [2,9,24] and newly obtained data, more than 30 ore minerals were identified in the Kalarskoe occurrence. Such diverse mineralogical composition, combined with complex geology, confounds genetic interpretations.

Based on geochemical and mineralogical observations (Table 9), we consider the Kalarskoe occurrence to be composed of the intermediate sulfidation (IS) type, according to the descriptions given in [7,25,26]. This includes widespread sulfide minerals (up to 40%) such as pyrite, arsenopyrite, sphalerite, and galena, as well as geochemical association with Au with Ag, Pb, Zn, and Te. The additional characteristics which are in favor of the IS type of mineralization include the veined morphology of the ore zones and their association with a predominantly calc-alkaline series of volcanic rocks which were formed on the Andean-type active margin. However, these conclusions must be additionally verified. Previous studies of Au-Ag occurrences and deposits located in the Devonian volcanogenic belt of the western part of the ASFA were identified as examples of low sulfidation (LS) [5] and high sulfidation (HS) types [3].

Table 9. Comparison of the obtained data (mineral composition of veins, altered rocks, mineralization style, volcanic rocks, and tectonic settings) from the Kalarskoe occurrence, along with the characteristics of various epithermal types, according to Refs. [7,25,26].

Type	Ore Minerals	Major Vein Minerals	Main Alteration Types	Main Mineralization Styles	Sulfide Abundance	Genetically Related Volcanism and Tectonic Settings
High sulfidation	Found: pyrite (common) Not found: enargite, luzonite, famatinite, covellite, tellurides	Found: quartz Not found: alunite, barite, vuggy residual quartz	Not found: silicification, quartz-alunite/APS, quartz-pyrophyllite/dickite at depth	Found: massive sulfide bodies, stockworks, hydrothermal breccias Not found: stockwork-disseminations and veins in massive and vuggy quartz	10–90 vol%	calc-alkaline andesitic-dacitic arcs (neutral stress to mildly extensional arc, compressive back arc during arc volcanism)
Intermediate sulfidation	Found: pyrite (common), arsenopyrite (common), chalcopyrite, sphalerite, galena, pyrrhotite, tetrahedrite-(Zn), tetrahedrite-(Fe) Not found: tellurides	Found: quartz, Mn carbonates (common), calcite Not found: barite, rhodonite, adularia	Found: quartz-sericite, quartz-illite	Found: veins, stockworks	5–30 vol%	calcic to calc-alkaline andesitic-dacitic volcanic-subvolcanic rocks: NC (neutral-compressional)-type and E (extensional)-type

Table 9. *Cont.*

Type	Ore Minerals	Major Vein Minerals	Main Alteration Types	Main Mineralization Styles	Sulfide Abundance	Genetically Related Volcanism and Tectonic Settings
Low sulfidation	Found: pyrite (common), arsenopyrite [1] (common), chalcopyrite, sphalerite [2], galena pyrrhotite [1], tetrahedrite-(Zn), tetrahedrite-(Fe) Not found: selenides	Found: quartz Not found: ankerite-dolomite, adularia, fluorite, barite, celestine, chalcedony	Not found: quartz-illite/smectite-adularia	Found: veins, stockworks, disseminations	1–5 vol% (but up to 20 vol% for basalt)	Bimodal volcanism (extensional settings: extensional intra-arc and back-arc, post-collisional orogenic belts, continental and island-arc rifts)

Found—characteristics of the Kalar occurrence coinciding with those of the epithermal type. Not found—undetected characteristics at the Kalar ore occurrence, however typical for the epithermal type. APS—aluminum-phosphate-sulfate minerals. [1] Minor to very minor minerals for LS type. [2] For IS type low-Fe sphalerite, for LS type high-Fe sphalerite.

The HS, and to a lesser extent, the IS deposits, show an association with porphyry copper systems [7,27,28]. Thus, multiphase Kistal syenogranite-granite-leucogranite pluton, which is located southwest of the Kalarskoe field (Figure 2), might be a subject of interest. The pluton cuts the Early Devonian volcanites of the Uchulensk-Kazankol formation, and its surface, according to geophysical data, sinks to the north and northeast. Mineralization zones possessing chalcopyrite and molybdenite, as well as Cu and Mo geochemical anomalies, are described within the massif and its exocontact zones. At a distance of 2–4 km from the Kistal pluton, there are Cu, Pb, and Zn geochemical anomalies. Farther north and northeast are located the Kalarskoe, Patyrin, and Nizhnekaz epithermal Au-Ag occurrences.

8.2. The Age of Au-Ag Mineralization

The geochronological data revealed a large scattering of ages within the Kalarskoe occurrence. The age of subvolcanic rhyolite porphyry bodies intruding into the volcanites of the Uchulen-Kazankol complex in the Kalarskoe site is 380 ± 2 Ma, while the age of the Au-Ag ores determined for sericite from the Au-bearing beresites with galena, arsenopyrite, and pyrite is 396 ± 4 Ma (Table 1). The (U,Th)-He age of pyrite (pyrite-3 and pyrite-4) from the Kalarskoe occurrence varies from ~399 to 371 Ma.

Most of the epithermal deposits are formed relatively fast, within the first millions of years [27]. Nevertheless, there are some deposits where several mineralization events of different ages can be distinguished. For example, for the Cerro Bayo District, Chilean Patagonia, the history of the epithermal mineralization spans 33 Myr [29]. The protracted formation of the epithermal mineralization is related to the pulses of magma and fluid generation due to continuous subduction.

In the case of the Kalarskoe occurrence, the time range obtained by the U-Pb and Ar-Ar systems is 16 Myr (Table 1), which is in a range of the timescales of continuous subduction magmatic activity [30]. Given the close ages of the volcano-sedimentary rocks in the area (415–375 Ma; [10]) and the (U,Th)-He ages of pyrite grains (399–371 Ma), we can propose that the epithermal mineralization within the Kalarskoe occurrence was synchronous to the volcanic activity and was formed in several episodes between ~400 to 371 Ma. The protracted history of ore formation might explain the variations in the ore mineral abundances and their diversity. More studies are required to confirm this suggestion.

9. Conclusions

There are several mineralized clusters with epithermal Au-Ag mineralization in the western part of ASFA that are located within the fragmented Devonian volcano-plutonic

belt of about 800 km long. The Au-Ag mineralization is confined predominantly to Early-Middle Devonian intermediate and felsic volcanic rocks, as well as to subvolcanic bodies of dacite and rhyolite composition. The most promising areas for prospecting are the epithermal Au-Ag deposits of the Kaburchak cluster, where the mineralization is related to the Uchulen-Kazankol complex (D_{1-2}). Within the most studied Kalarskoe occurrence the mineralized bodies are confined to linear zones of intense silicification, sulfidization, quartz-sulfide veins, and veinlets within the low-temperature metasomatic rocks. Au-Ag mineralization is marked by geochemical halos and anomalies of Au, Ag, Pb, Zn, As, Sb, and Hg. There is a clear positive correlation of Au with Ag, As, Bi, Sb, and Pb.

Volcanic rocks and subvolcanic bodies of the Kalarskoe occurrence were altered by metasomatic processes, which resulted in the formation of propylites and imposed argillic-altered rocks on them. The argillic-altered rocks host the widespread arsenopyrite-pyrite mineralization, along with numerous veinlets and veins, predominantly of sulfide-quartz composition. Characteristic features of the mineralized bodies are the high content of the ore minerals (10%–20% and in some cases, up to 75%) and a variety of mineral forms, including the wide distribution of variable compositions of sulfosalts of Pb, Bi, Ag, and Cu, Ag-containing fahlores, electrum, native Au, and tellurides of Au, Ag, and Pb. Based on geochemical and mineralogical data, it can be assumed that the Au-Ag mineralization of the Kalarskoe occurrence belongs to the IS type.

The age of Au-Ag mineralization is determined by a close association with Early-Middle Devonian volcanic rocks and the results of the geochronological studies. The dating of pyrite from ores of the Kalarskoe occurrence using the (U,Th)-He method, combined with U-Pb and Ar-Ar data, allowed us to establish the protracted mineralization history, with a wide range of age values from ~370 to 400 Ma.

The epithermal Au-Ag mineralization shows a regional distribution in the western part of the ASFA, and given that the region is poorly studied, the area can be considered promising for identifying new deposits. The obtained results significantly complement the prospecting models for epithermal Au-Ag deposit exploration in the western part of the ASFA and will contribute to their more effective prospecting.

Supplementary Materials: The following supporting information can be downloaded at: https://www.mdpi.com/article/10.3390/min14070708/s1; Supplementary Material File S1: The Devonian Kalar epithermal occurrence of the Kaburchak Au-Ag cluster, Altai-Sayan Folded Belt, Russia: geological setting, mineralogical, geochemical, and geochronological features; Supplementary Material File S2: Interpretation of the (U,Th)-He ages, References [31–33] are cited in the Supplementary Materials.

Author Contributions: Conceptualization: A.I.C., E.A.N., P.N.L. and O.V.Y.; methodology: A.I.C., P.N.L., O.V.Y. and L.A.S.; validation: A.I.C., E.A.N., P.N.L. and O.V.Y.; formal analysis: P.N.L., L.A.S., M.O.A. and O.V.Y.; investigation: A.I.C., P.N.L., L.A.S. and O.V.Y.; resources: A.I.C., E.A.N. and P.N.L.; writing—original draft preparation: A.I.C., E.A.N., P.N.L., O.V.Y. and L.A.S.; writing—review and editing, A.I.C., E.A.N. and O.V.Y.; visualization: P.N.L., A.I.C., E.A.N. and L.A.S.; supervision: A.I.C., E.A.N. and O.V.Y.; project administration: E.A.N.; funding acquisition: A.I.C., E.A.N. and O.V.Y. All authors have read and agreed to the published version of the manuscript.

Funding: The (U:Th)-He dating of pyrite was funded by Russian Science Foundation, grant number 22-77-10088. The chemical analyses, performed by M.O. Anosova, were funded by the State Assignment of the Vernadsky Institute of Geochemistry and Analytical Chemistry RAS.

Data Availability Statement: The data supporting the reported results can be obtained by request to naumov@tsnigri.ru.

Acknowledgments: The authors are grateful to the Rosgeo JSC for the opportunity to work with the core samples; to S.G. Kryazhev, E.V. Kovalchuk, and P.Yu. Plechov for their assistance in the mineralogical studies; and to B.M. Gorokhovskiy for helium lab assistance.

Conflicts of Interest: A.I. Chernykh is employed by the PJSC Polyus Company. The paper reflects the views of the scientists and not the company. The authors declare no conflicts of interest. The funders had no role in the design of the study; in the collection, analyses, or interpretation of data; in the writing of the manuscript; or in the decision to publish the results.

References

1. Chernykh, A.I.; Nevolko, P.A.; Borisenko, A.S. Epithermal Au-Ag Mineralization of the Kaburchak Ore Cluster (Gornaya Shoria)—Localization Features, Mineralogy and Age. *Geol. Miner. Resour. Sib.* **2013**, *3*, 76–82. (In Russian)
2. Chernykh, A.I.; Brysin, M.P.; Leibgam, P.N.; Arsentyeva, I.V.; Milyaev, S.A. Mineralogical Features of the Ores of the Kalarskoe Occurence and the Possibilities of the Ion-Sorption Method for Searching for Overlain Au-Ag Mineralization in the Altai-Sayan Folded Region. *Geol. Miner. Resour. Sib.* **2020**, *3*, 87–99. (In Russian)
3. Gusev, N.I.; Gusev, A.I.; Shokalsky, S.P. Mesozoic tectonothermal activation and epithermal gold mineralization in the northeastern Altai Mountains. *Russ. Reg. Geol. Metallog.* **2014**, *57*, 49–67. (In Russian)
4. Babin, G.A.; Shokalsky, S. Main Features of the Geological Structure of the Altai-Sayan Folded Region (Tectonic Zoning, Stratigraphy, Magmatism, History of Geological Development). *Geol. Miner. Resour. Sib.* **2017**, *6*, 19–37. (In Russian)
5. Gusev, N.I.; Shokalsky, S.P.; Gusev, A.I. Age of Magmatism (U-Pb, SHRIMP II), Controlling Epithermal Mineralization of the Novofirsovo Au Ore Cluster (Altai). *Russ. Reg. Geol. Metallog.* **2011**, *45*, 98–105. (In Russian)
6. Chernykh, A.I. Prediction of epithermal gold-silver mineralization in the Altai-Sayany folded region based on correlation with reference objects of northwestern Pacific. In Proceedings of the International Geology and Mining Forum, Magadan, Russia, 3–5 September 2011; pp. 233–234.
7. Sillitoe, H.R.; Hedenquist, W.J. Linkages between Volcanotectonic Settings, Ore-Fluid Compositions, and Epithermal Precious Metal Deposits. In *Volcanic, Geothermal, and Ore-Forming Fluids*; Society of Economic Geologists: Littleton, CO, USA, 2005; Volume 10, pp. 315–343.
8. Gusev, A.I. Epithermal mineralization of precious metals in Gorny Altai and Gorny Shoria. *Izv. Tomsk Polytech Univ. Nauk. Zemle* **2005**, *308*, 32–35. (In Russian)
9. Leibham, P.N. Au-Ag mineralization of the Kalar orefield, Gornaya Shoriya, Russia. In Proceedings of the 16th SGA Biennial Meeting, Rotorua, New Zealand, 28–31 March 2022; pp. 192–195.
10. Varenik, A.V. *Exploration Work for Au-Ag Mineralization within the Promising Areas of the Krasnogorsk-Kaburchak Area (Kemerovo Region)*; СНИИГиМС: Novosibirsk, Russia, 2020. (In Russian)
11. Chernykh, A.I. Geological-mineragenic mapping for gold at a scale of 1:500000 of the northwestern part of the Altai-Sayan folded region (tasks, methods, results). *Izv. Tomsk Polytech Univ. Nauk. Zemle* **2009**, *314*, 16–22. (In Russian)
12. Gerachenko, A.A. *Analys of the Mineral Resources Base of the Kemerovo District*; Federal Agency for Subsoil Management: Moscow, Russia, 2000. (In Russian)
13. Reed, S.J.B. *Electron Microprobe Analysis and Scanning Alectron Microscopy in Geology*; University of Cambridge: Cambridge, UK, 2005; ISBN 978-0-511-12414-3.
14. Yakubovich, O.V.; Gedz, A.M.; Vikentyev, I.V.; Kotov, A.B.; Gorokhovskii, B.M. Migration of Radiogenic Helium in the Crystal Structure of Sulfides and Prospects of Their Isotopic Dating. *Petrology* **2019**, *27*, 59–78. [CrossRef]
15. Yakubovich, O.; Podolskaya, M.; Vikentyev, I.; Fokina, E.; Kotov, A. U-Th-He geochronology of pyrite from the Uzelga VMS deposit (South Urals)—New perspectives for direct dating of the ore-forming processes. *Minerals* **2020**, *10*, 629. [CrossRef]
16. Yakubovich, O.; Vikentyev, I.; Ivanova, E.; Podolskaya, M.; Sobolev, I.; Tyukova, E.; Kotov, A. U-Th-He Geochronology of Pyrite from Alteration of the Au-Fe-Skarn Novogodnee-Monto Deposit (Polar Urals, Russia)—The Next Step in the Development of a New Approach for Direct Dating of Ore-Forming Processes. *Geosciences* **2021**, *11*, 408. [CrossRef]
17. Shukolyukov, Y.A.; Yakubovich, O.V.; Mochalov, A.G.; Kotov, A.B.; Sal'nikova, E.B.; Yakovleva, S.Z.; Korneev, S.I.; Gorokhovskii, B.M. New geochronometer for the direct isotopic dating of native platinum minerals (190Pt-4He method). *Petrology* **2012**, *20*, 491–505. [CrossRef]
18. Vermeesch, P. IsoplotR: A free and open toolbox for geochronology. *Geosci. Front.* **2018**, *9*, 1479–1493. [CrossRef]
19. Moëlo, Y.; Makovicky, E.; Mozgova, N.N.; Jambor, J.L.; Cook, N.; Pring, A.; Paar, W.; Nickel, E.H.; Graeser, S.; Karup-Møller, S.; et al. Sulfosalt systematics: A review. Report of the sulfosalt sub-committee of the IMA Commission on Ore Mineralogy. *Eur. J. Mineral.* **2008**, *20*, 7–46. [CrossRef]
20. Mozgova, N.N. *Nonstoichiometry and Homologous Series of Sulfosalts*; Marfunin, A.S., Ed.; Nauka: Moscow, Russia, 1985. (In Russian)
21. Barrie, C.D.; Pearce, M.A.; Boyle, A.P. Reconstructing the pyrite deformation mechanism map. *Ore Geol. Rev.* **2011**, *39*, 265–276. [CrossRef]
22. Vikentyev, I.V.; Belogub, E.V.; Novoselov, K.A.; Moloshag, V.P. Metamorphism of volcanogenic massive sulphide deposits in the Urals. Ore geology. *Ore Geol. Rev.* **2017**, *85*, 30–63. [CrossRef]
23. Chernyshev, I.; Konečný, V.; Lexa, J.; Kovalenker, V.A.; Jeleň, S.; Lebedev, V.A.; Goltsman, Y.V. K-Ar and Rb-Sr Geochronology and Evolution of the Štiavnica Stratovolcano (Central Slovakia). *Geol. Carpathica* **2013**, *64*, 327–351. [CrossRef]
24. Sillitoe, R.H. Epithermal Paleosurfaces. *Miner. Depos.* **2015**, *50*, 767–793. [CrossRef]

25. Wang, L.; Qin, K.-Z.; Song, G.-X.; Li, G.-M. A review of intermediate sulfidation epithermal deposits and subclassification. *Ore Geol. Rev.* **2019**, *107*, 434–456. [CrossRef]
26. Sillitoe, H.R. Porphyry Copper Systems. *Econimic Geol.* **2010**, *105*, 3–41. [CrossRef]
27. Nikolaev, Y.N.; Baksheev, I.A.; Prokofiev, V.Y.; Nagornaya, E.V.; Marushchenko, L.I.; Sidorina, Y.N.; Chitalin, A.F.; Kal'ko, I.A. Au–Ag Mineralization in Porphyry–Epithermal Systems of the Baimka Trend, Western Chukchi Peninsula, Russia. *Geol. Ore Depos.* **2016**, *58*, 284–307. [CrossRef]
28. Poblete, J.A.; Bissig, T.; Mortensen, J.K.; Gabites, J.; Friedman, R.; Rodriguez, M. The Cerro Bayo District, chilean patagonia: Late Jurassic to cretaceous magmatism and protracted history of epithermal Ag-Au mineralization. *Econ. Geol.* **2014**, *109*, 487–502. [CrossRef]
29. Lee, C.T.A.; Anderson, D.L. Continental crust formation at arcs, the arclogite "delamination" cycle, and one origin for fertile melting anomalies in the mantle. *Sci. Bull.* **2015**, *60*, 1141–1156. [CrossRef]
30. Buslov, M.M.; Travin, A.V.; Kulikova, A.V.; Semakov, N.N.; Rubanova, E.S.; Abildaeva, M.A.; Trofimova, D.A.; Geng, H.; Ming, C.; Otgonbaatar, D.; et al. Tectonics and Geodynamics of Gorny Altai and Adjacent Structures of the Altai-Sayan Folded Belt. *Russ. Geol. Geophys.* **2013**, *54*, 1600–1627. (In Russian) [CrossRef]
31. Stuart, F.M.; Duckworth, R.; Turner, G.; Schofield, P.F. Helium and sulfur isotopes of sulfide minerals from Middle valley. *Proc. Ocean Drill. Progr. Sci. Results* **1994**, *139*, 387–392.
32. Farley, K.A.; Wolf, R.A.; Silver, L.T. The effects of long alpha-stopping distances on (U-Th)/He ages. *Geochim. Cosmochim. Acta* **1996**, *60*, 4223–4229. [CrossRef]
33. Flowers, R.M.; Zeitler, P.K.; Danišík, M.; Reiners, P.W.; Gautheron, C.; Ketcham, R.A.; Metcalf, J.R.; Stockli, D.F.; Enkelmann, E.; Brown, R.W. (U-Th)/He chronology: Part 1. Data, uncertainty, and reporting. *GSA Bull.* **2022**, *135*, 104–136. [CrossRef]

Disclaimer/Publisher's Note: The statements, opinions and data contained in all publications are solely those of the individual author(s) and contributor(s) and not of MDPI and/or the editor(s). MDPI and/or the editor(s) disclaim responsibility for any injury to people or property resulting from any ideas, methods, instructions or products referred to in the content.